INVESTIGATING NEW REACTIONS FOR COORDINATED DINITROGEN

by

ROSA PARK

B. Sc. (Hons.), York University, 2005

A thesis submitted in partial fulfillment of
the requirements for the degree of

MASTER OF SCIENCE

in

THE FACULTY OF GRADUATE STUDIES

(CHEMISTRY)

THE UNIVERSITY OF BRITISH COLUMBIA
(VANCOUVER)

April 2008

© Rosa Park, 2008

Abstract

The chemistry of the tantalum dinitrogen complex ([NPN]Ta)$_2$(μ-H)$_2$(μ-η^1:η^2-N$_2$)Ta-[NPN], **1**, (where [NPN] represents the acyclic tridentate ligand [(PhNSiMe$_2$CH$_2$)$_2$-PPh]$^{2-}$), with primary alkenes, group IV and V metallocene complexes, and GaCp* is explored.

The reaction of **1** with 1-pentene and 1-hexene occurs via olefin-insertion into the metal-hydride bond to give two new complexes, ([NPN]Ta(CH$_2$)$_4$CH$_3$)$_2$(μ-η^1:η^1-N$_2$), **10**, and ([NPN]Ta(CH$_2$)$_5$CH$_3$)$_2$(μ-η^1:η^1-N$_2$), **11**, which were characterized using NMR spectroscopy. The solid-state structure of **11** was established and revealed that N$_2$ has been transformed into a bridging end-on mode. In contrast to its C_s symmetry in solution, the solid-state structure of **11** is C_i symmetric; a VT-NMR study was performed and showed that **11** exists as an equilibrium between two isomers in solution: a C_s symmetric isomer **11A**, which is the predominant isomer at room temperature, and a C_i symmetric isomer **11B**, which is the minor isomer.

The reactivity of **1** with group IV and V metallocenes was investigated. The reaction of **1** with Cp$_2$Hf(PMe$_3$)(η^2-Me$_3$SiCCSiMe$_3$) produces [N(μ-P=N)N]Ta(μ-H)$_2$(μ-N(Hf-Cp$_2$))Ta[NPN], **14**, in which N$_2$ is cleaved and new Hf-N and P=N bonds have formed. The reaction of **1** with group V metallocene hydrides Cp$_2$MH$_3$ (M = Nb, Ta) was also attempted however these complexes do not react with **1**.

The reaction of **1** with GaCp* produces a new complex, [NPN]Ta(μ-N(GaCp*))Ta(=NPh)[NPμ-N], **18**, which was characterized using NMR spectroscopy. Complex **18** decomposes over several days in solution, and one product of decomposition

that was isolated was $[(PhNH)(NP\mu\text{-}N)Ta]_2$, **19**. The solid-state structure of **19** showed that the [NPN] ligand was cleaved at the N-Si bond, similar to that observed for the reaction of **1** with 9-BBN and $HB(C_6H_5)_2$. A mechanism for the formation of complexes **18** and **19** is proposed.

Table of Contents

Abstract....ii
Table of Contents....iv
List of Tables....vi
List of Figures....vii
Glossary of Terms....x
Acknowledgements....xiii
Dedication....xiv

Chapter 1: The Chemistry of Dinitrogen

1.1 Introduction....1
1.2 Nitrogen Fixation and the Haber-Bosch Process....5
1.3 The Chemistry of Side-on End-on Dinitrogen....7
1.4 Scope and Prospectus....14

Chapter 2: Olefin Insertion Reactions of the Side-on End-on Dinitrogen Complex

2.1 Introduction....15
2.2 Olefin Insertion Reactions....17
2.2.1 Olefin Insertion Reactions of Bridging Hydride Complexes....18
2.2.2 Hydrozirconation of Olefins....20
2.2.3 Olefin Insertion with **1**....22
2.3 Results and Discussion....23
2.3.1 Reaction of **1** with 1-pentene....23
2.3.2 Reaction of **1** with 1-hexene....26
2.4 Conclusions....33
2.5 Experimental....33
2.5.1 General Procedure....33
2.5.2 Materials and Reagents....34
2.5.3 Synthesis, Characterization, and Reactivity of Complexes....35

Chapter 3: The Reactivity of Group IV and V Metallocenes with Side-on End-on Coordinated N_2

3.1 Introduction....39

3.2 The Chemistry of Cp_2NbH_3 and Cp_2TaH_3....42

3.3 The Reaction of 1 with $Cp_2Zr(II)$ and $Cp_2Ti(II)$....44

3.4 Results and Discussion....47

3.4.1 Reaction of **1** with $Cp_2Hf(PMe_3)(\eta^2\text{-}Me_3SiCCSiMe_3)$....47

3.4.2 Attempted Reaction of **1** with Cp_2NbH_3 and Cp_2TaH_3....50

3.5 Conclusions....51

3.6 Experimental....52

2.6.1 General Procedure....52

3.6.2 Materials and Reagents....52

3.6.3 Synthesis, Characterization, and Reactivity of Complexes....52

Chapter 4: The Reactivity of a Group 13 Complex with Side-on End-on Coordinated N_2

4.1 Introduction....55

4.2 The Reaction of **1** with Lewis Acids....57

4.3 Results and Discussion....58

4.3.1 Reaction of **1** with GaCp*....58

4.4 Conclusions....65

4.5 Summary and Future Work....65

4.6 Experimental....67

4.6.1 General Procedure....67

4.6.2 Materials and Reagents....67

4.6.3 Synthesis, Characterization, and Reactivity of Complexes....67

4.7 References....69

Appendix: X-ray Crystal Structure Data

A1 Crystallographic Data....77

List of Tables

Table 1.1 N-N bond lengths and stretching frequencies for some simple molecules and N_2 complexes.....2

Table 1.2 The different bonding modes of N_2 in mono- and bimetallic transition metal (M) complexes.....4

Table 1.3 A comparison of selected bond lengths (Å) for **1** and **2**.....10

Table 3.1 Group IV and V metallocene N_2 complexes, their precursors and N-N bond lengths (Å).....42

Table A-1 Crystallographic Data and Structure Refinement for $([NPN]Ta)_2(\mu\text{-}H)_4$ (**2**) and $([NPN]Ta(CH_2)_5CH_3)_2(\mu\text{-}\eta^1\text{:}\eta^1\text{-}N_2)$ (**11**).....77

Table A-2 Crystallographic Data and Structure Refinement for $[N(\mu\text{-}P{=}N)N]Ta(\mu\text{-}H)_2(\mu\text{-}N(HfCp_2))Ta[NPN]$ (**14**) and $[(PhNH)(NP\mu\text{-}N)Ta]_2$ (**19**).....78

List of Figures

Figure 1.1 Some examples of activated early transition metal N_2 complexes and their N-N bond lengths.....3

Figure 1.2 Structure of the FeMo cofactor extracted from the nitrogenase enzyme in *Azotobacter vinelandii*.....6

Figure 1.3 ORTEP depiction of the solid-state molecular structure of **2**.....9

Figure 2.1 An illustration of the four-centered transition state formed in an olefin-hydride insertion.....15

Figure 2.2 Examples of hydride-olefin complexes and the activation energies (kcal/mol) associated with the hydride-insertion into ethylene.....16

Figure 2.3 Two complexes in which the hydride and olefin ligands are *cis*.....17

Figure 2.4 Subsequent reactions of $Cp_2Zr(R)Cl$.....21

Figure 2.5 $^{31}P\{^{1}H\}$ NMR spectrum of **10** in C_6D_6.....24

Figure 2.6 300 MHz ^{1}H NMR spectrum of **10** in C_6D_6.....24

Figure 2.7 $^{13}P\{^{1}H\}$ NMR spectrum of **10**-$^{15}N_2$.....25

Figure 2.8 $^{15}N\{^{1}H\}$ NMR spectrum of **10** in C_6D_6.....26

Figure 2.9 $^{15}N\{^{1}H\}$ NMR spectrum of **11** in C_6D_6.....27

Figure 2.10 ORTEP depiction of the solid state molecular structure **11**....28

Figure 2.11 A stack plot of $^{31}P\{^{1}H\}$ NMR spectra of **11** from 273 K to 203 K.....30

Figure 2.12 Van't Hoff plot of **11** from 283 K to 203 K.....31

Figure 3.1 Examples of side-on and end-on N_2 metallocene complexes.....40

Figure 3.2 A group V metallocene hydride.....43

Figure 3.3 $^{31}P\{^{1}H\}$ NMR spectrum of **14** in C_6D_6.....48

Figure 3.4 An ORTEP depiction of the solid-state molecular structure of **14**.....49

Figure 4.1 $^{31}P\{^{1}H\}$ NMR spectrum of **1** and GaCp* in C_6D_6.....59

Figure 4.2 $^{31}P\{^{1}H\}$ NMR spectrum of **18** in C_6D_6.....60

Figure 4.3 400 MHz ^{1}H NMR spectrum of **18** in C_6D_6.....61

Figure 4.4 $^{15}N\{^{1}H\}$ NMR resonances of **18** in C_6D_6.....62

Figure 4.5 An ORTEP depiction of the solid-state molecular structure of **19**.....63

Glossary of Terms

Å	Angström (10^{-10} m)
Anal.	analysis
atm	atmosphere
9-BBN	9-borabicyclononane $(HB(C_8H_{14}))_2$
^{i}Bu	isobutyl group ($-CH_2CH(CH_3)_2$)
^{n}Bu	normal butyl group ($-CH_2CH_2CH_2CH_3$)
^{t}Bu	tertiary butyl group ($-C(CH_3)_3$)
°C	degrees Celsius
^{13}C	carbon -13
Calcd.	calculated
cm^{-1}	reciprocal centimeters (wavenumbers)
COSY	correlated spectroscopy
Cp	cyclopentadienyl group ($[C_5H_5]^-$)
Cp*	pentamethylcyclopentadienyl group ($[C_5Me_5]^-$)
DIBAL	diisobutylaluminium hydride $(HAl(CH_2CH(CH_3)_2)_2$
d	doublet
D	deuterium
2D	two-dimensional
δ	delta
Δ	heat
dd	doublet of doublets
deg (°)	degrees
DFT	density functional theory
dppe	*bis*(diphenylphosphino)ethane
E_a	Activation Energy
equiv	equivalent
g	grams
HIPT	hexa-isopropylterphenyl substituent

HOMO	Highest Occupied Molecular Orbital
HSQC	Heteronuclear Single Quantum Coherence
Hz	Hertz
$^{n}J_{AB}$	coupling constant between nuceli A and B over n bonds
K	degrees Kelvin
kcal	kilocalories
kJ	kilojoules
L	ligand group
LUMO	Lowest Unoccupied Molecular Orbital
M	metal
M-H	metal hydride
Me	methyl substituent
m	multiplet
m	*meta*-position of aryl ring
mg	milligrams
MgADP	adenosine diphosphate, magnesium salt
MgATP	adenosine triphosphate, magnesium salt
mol	mole
mmol	millimoles
MOs	molecular orbitals
^{15}N	nitrogen-15
nm	nanometer
NMR	nuclear magnetic resonance
[NPN]	$[PhP(CH_2SiMe_2NPh)_2]^{2-}$
η^n	hapticity of order n
o	*ortho*-position of aryl ring
ORTEP	Oakridge Thermal Ellipsoid Plotting Program
p	*para*-position of aryl ring
^{31}P	phosphorous-31
Ph	phenyl group ($-C_6H_5$)
π	pi

ppm	parts per million
py	pyridine group
^{i}Pr	isopropyl group (-CH(CH_3)$_2$)
R	alkyl or aryl group
rt	room temperature
s	singlet
σ	sigma
t	triplet
T	temperature
THF	tetrahydrofuran
TMS	tetramethylsilane ((CH_3)$_4$Si)
ν_{NN}	stretching freqency of N-N bond
X	halide group
Z	number of formula units in the unit cell

Acknowledgements

I would like to thank Professor Mike Fryzuk for giving me the opportunity to work in this group, and inspiring me with dinitrogen chemistry. His patience, encouragement and support were instrumental throughout my time at U.B.C.

To my labmates, for all the fun beer drinking memories and insightful discussions, both chemistry related and otherwise; Fiona Hess, Bryan Shaw, Gabriel Menard, Kyle Parker, Nathan Halcovitch, Joerg Schachner, Owen Summerscales, and Yasuhiro Ohki. Special thanks are due to Howie Jong and M.J. Ferreira for solving the X-ray structures. Thank-you Dr. Erin MacLachalan for editing this entire thesis while being a full-time mommy - your comments and suggestions were invaluable in writing this thesis.

Many thanks to the excellent staff at the Chemistry Department at U.B.C.: Ken Love and Milan for the countless hours in fixing and maintaining the old glove box - its old but still going strong; Zorana Danilovic, Maria Ezhova, Nick Burlinson, Andrew Lewis (at S.F.U.), and Colin Zhang (at S.F.U.) and for all of their support with NMR spectroscopy; Brian Ditchburn for fixing my line and glassblowing all of the sealed NMR tubes and broken J-Young tubes; Noga Levit for being a great safety advisor; Brian Patrick for his expertise with the X-ray structures; Sophia Nussbaum for allowing me to TA the first year labs, and introducing me to Bucky; everyone at chem stores, mech shop and electronics shop - thank you.

To my family: mom, dad, grandma, and grandpa, thank you for always encouraging me to do my best and having faith in everything I do; to my dear sisters, Domina and Agnes for being my cheerleaders - I love you guys! Thank you Sharon Lee, Haidy Abdel-Sayed and Michel Yun for being an incredible support group and being there for me whenever I was homesick.

Dedication

For my family - mom, dad, grandma, grandpa, Agnes and Domina - I am truly blessed to have such a loving family.

Chapter One

The Chemistry of Dinitrogen.

1.1 Introduction.

The earth's atmosphere is composed of about 78% N_2.[1] Reduced nitrogen is found in many biologically relevant compounds such as amines, nucleic acids and proteins, and nitrogen is an essential element for all life forms.[2] However, despite its abundance, N_2 is extremely inert, and the challenge in trying to use transition-metal complexes to catalytically activate and functionalize N_2 still remains.

Using N_2 as a reagent industrially is appealing because it is abundant, accessible, and inexpensive; the development of a transition-metal catalyst that can convert N_2 into nitrogen-containing compounds such as amines or N-heterocycles would be ideal. However, the intrinsic properties of N_2 are a barrier to attaining such a cycle, so far. In contrast to isoelectronic carbon monoxide, which is a reactive molecule and an excellent ligand, N_2 is incredibly stable and a poor ligand.[3] The reasons for its stability are: it is non polar, it has a high bond dissociation enthalpy (945 kJ mol^{-1}), as well as a large HOMO-LUMO gap.[4] All of these properties make it difficult for N_2 to bind to transition metals, and to be oxidized or reduced.

When dinitrogen does bind to a metal complex it may become activated, and the degree of activation can be correlated from the N-N bond length (typically determined by X-ray diffraction), or by the stretching frequency of N_2 in the complex (determined by infrared or Raman spectroscopy). A comparison of N-N bond lengths of some organic compounds,

along with some examples of dinitrogen complexes is given in Table 1.1. Stretching frequencies determined by IR and Raman are also included, if data was available.

Table 1.1. N-N bond lengths and stretching frequencies (R = Raman, IR = Infrared) for some simple molecules, as well as for some dinitrogen metal complexes.

Compound	N-N bond Length (Å)	N-N Stretching Frequency (cm^{-1})
$N_{2(g)}$ [5]	1.0975	2331 (R)
PhN=NPh [6]	1.255	1442 (R)
$H_2N\text{-}NH_2$ [7]	1.449	1111 (R)
$CpFe(dippe)(N_2)^+$ [8]	1.13(1)	2112 (IR)
$\{[Pr^i_2PCH_2SiMe_2)_2N]Zr(Cl)\}_2(\mu\text{-}\eta^2\text{:}\eta^2\text{-}N_2)$ [9]	1.548(7)	731 (R)
$[(\eta^5\text{-}C_5H_2\text{-}1,2,4\text{-}Me_3)_2Ti]_2(\mu_2,\eta^2,\eta^2\text{-}N_2)$ [10]	1.216(3)	
$\{[(Me_3Si)_2N]_2(THF)Y\}_2(\mu,\eta^2\text{:}\eta^2\text{-}N_2)$ [11]	1.268(3)	
$\{Cp^*Ta[N(^iPr)C(Me)N(^iPr)]\}_2(\mu\text{-}\eta^1\text{:}\eta^1\text{-}N_2)$ [12]	1.288(10)	
$(^tBuNSiMe_2N(CH_2CH_2P^iPr_2)_2Mn)_2(\mu\text{-}\eta^1\text{:}\eta^1\text{-}N_2)$ [13]	1.208(6)	1685 (R)
$[Ir\{C_6H_3\text{-}2,6\text{-}(CH_2PBu^t_2)_2\}]_2(\mu\text{-}\eta^1\text{:}\eta^1\text{-}N_2)$ [14]	1.176(13)	
$[(\eta^5C_5Me_4H)_2Zr]_2(\mu\text{-}\eta^2\text{:}\eta^2\text{-}N_2)$ [15]	1.377(3)	
$[\{[(CH_2)_5C(\alpha\text{-}C_4H_2N)]_4\}Sm_3Li_2](\mu\text{-}\eta^2\text{:}\eta^2N_2)[Li(THF)_2]\text{-}(THF)_2$ [16]	1.502(5)	
$[(\eta^5C_5Me_4H)_2Hf]_2(\mu\text{-}\eta^2\text{:}\eta^2\text{-}N_2)$ [17]	1.423(11)	

The degree of N_2 activation in a complex depends on the identity of the metal, and its oxidation state, as well as on the nature of the ligands in the complex.[18] Early transition metal N_2 complexes typically display a greater degree of activation, while late transition metal N_2 complexes usually contain weakly activated nitrogen.[4] Some examples[19-23] of

activated early transition metal N_2 complexes, along with their bond lengths (measured by single crystal X-ray diffraction) are shown in Figure 1.1.

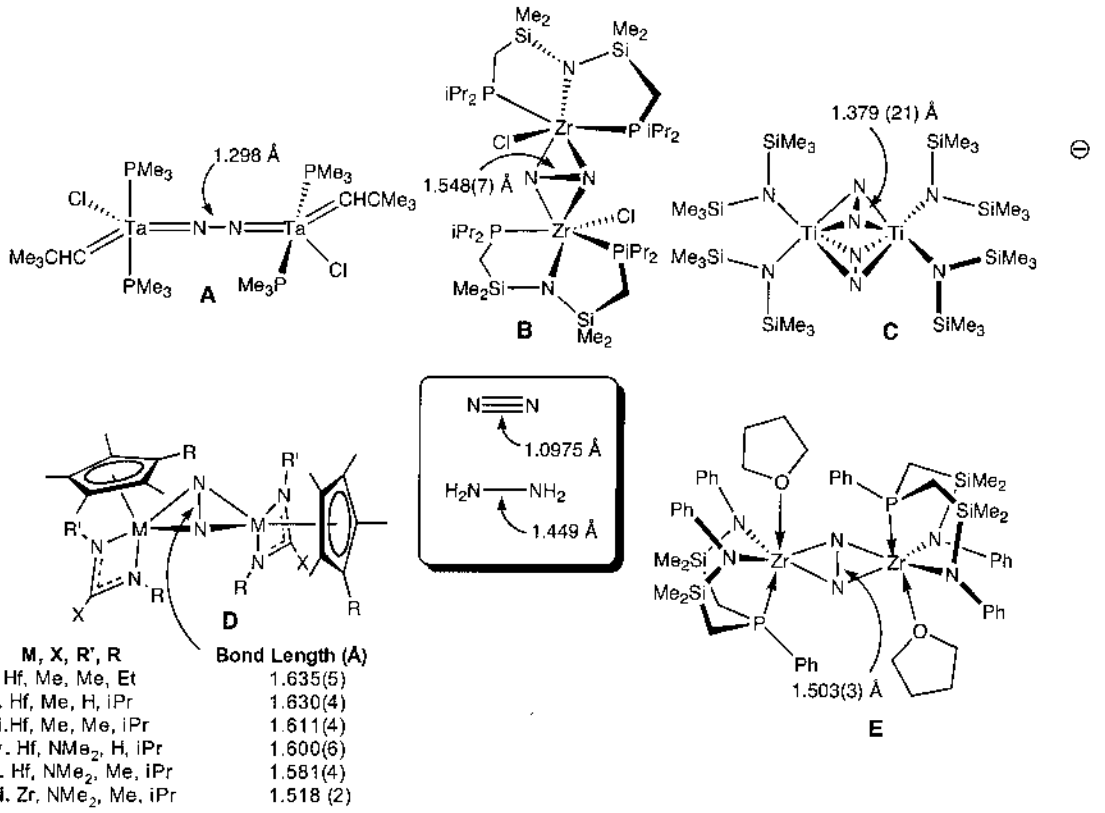

M, X, R', R	Bond Length (Å)
i. Hf, Me, Me, Et	1.635(5)
ii. Hf, Me, H, iPr	1.630(4)
iii. Hf, Me, Me, iPr	1.611(4)
iv. Hf, NMe_2, H, iPr	1.600(6)
v. Hf, NMe_2, Me, iPr	1.581(4)
vi. Zr, NMe_2, Me, iPr	1.518 (2)

Figure 1.1. Some examples of activated early transition metal N_2 complexes and their N-N bond lengths. For comparison, the bond lengths of dinitrogen and hydrazine are provided in the inset.

In Figure 1.1, N_2 activation is evident from the increased length of the N-N bond, which either approaches or exceeds the N-N single bond in hydrazine. The various complexes from structure **D** show even more dramatic lengthening of the N_2 bond;[22] end-on hafnium and zirconium complexes have N-N bond lengths that range from 1.518(2) to

1.635(5) Å (structures **Di** - **Dvi** in Figure 1.1). Complex **Di** has an N_2 bond length that is 1.635(5) Å, and is the longest N-N bond measured to date for an N_2 complex.[22]

The various binding modes of dinitrogen for both monometallic and bimetallic complexes, and the degree of N_2 activation are summarized in Table 1.2. The common bonding mode for transition metal dinitrogen complexes is end-on in both bimetallic and monometallic N_2 complexes.[24] It was not until 1988 when the first planar side-on bound N_2 complex $(Cp^*_2Sm)_2(\mu\text{-}\eta^2\text{-}\eta^2\text{-}N_2)$ was communicated.[25] Since 1988, many other side-on bound dinitrogen complexes have been reported, all of which have been structurally characterized as dinuclear metal systems, with the exception of one side-on monometallic N_2 complex, $[Os(NH_3)_5N_2][PF_6]_2$.[26]

Table 1.2. The different bonding modes of N_2 in mono- or bimetallic transition metal (M) complexes. Only connectivity is indicated, with approximations in bond order and N_2 activation (N-N triple bond = weak activation, N-N single bond = strong activation).

Weak Activation	Strong Activation	
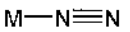		End-on Mononuclear
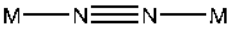	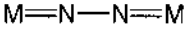	End-on Dinuclear
		Side-on Mononuclear
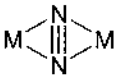	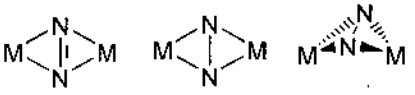	Side-on Dinuclear
		Side-on End-on Dinuclear

1.2 Nitrogen Fixation and the Haber-Bosch Process.

In 1965, Allen and Senoff reported the first transition metal dinitrogen complex, $[Ru(NH_3)_5N_2]^{2+}$, which resulted from the reaction of $RuCl_3$ with hydrazine hydrate, as shown in Equation 1.1.[27]

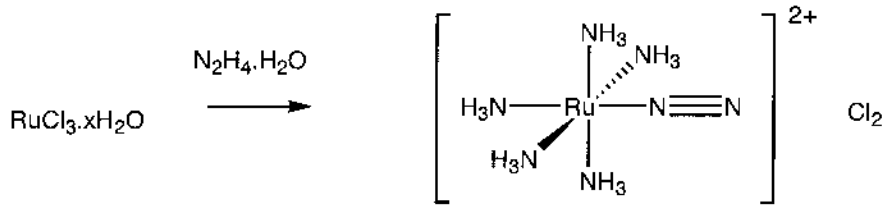

Equation 1.1.

Since this discovery, the coordination chemistry of N_2 has flourished. Some of this chemistry focused on modeling the active site in the nitrogenase enzyme, which converts N_2 into ammonia, in a process known as nitrogen fixation (Equation 1.2).[4]

$$N_{2(g)} + 8H^+ + 8e^- + 16MgATP \rightarrow 2NH_{3(g)} + H_{2(g)} + 16MgADP + 16P_i$$

Equation 1.2

Nitrogen fixation is carried out by certain bacteria, including *Azotobacter vinelandii* and *Clostridium pasteurianum*,[28] and produces thousands of tons of ammonia every day worldwide, (an estimated 170 x 10^6 tons/year) under ambient conditions (20°C, 1 atm).[29] The active site in nitrogenase, where N_2 is reduced to NH_3, is an iron-sulfur-molybdenum cofactor, or FeMoco.[4] A high-resolution crystallographic analysis of nitrogenase determined

at 1.16 Å was performed in 2002, and revealed a light atom (X) in the centre of FeMoco (shown in Figure 1.2), that is compatible with being C, N, or O.[30]

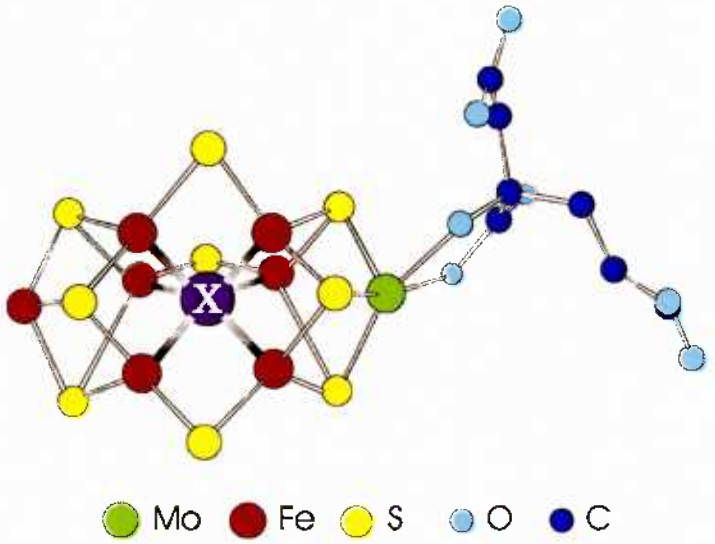

Figure 1.2. Structure of the FeMo cofactor extracted from the nitrogenase enzyme in *Azotobacter vinelandii*.[36]

The identity of atom X in the centre of the cofactor remains elusive. Although theoretical investigations suggested that X is a nitrogen atom,[31-34] recent experimental evidence does not support these claims.[35] Despite the fact that the structure of FeMoco has been scrutinized in great detail, the mechanism by which it transforms N_2 to NH_3 is still unclear.

N_2 is converted into ammonia industrially via the Haber-Bosch process.[37] In this process, N_2 reacts with three equivalents of H_2 to yield NH_3 under high temperature (400-550 °C) and pressure (270 atm) in the presence of an activated iron or ruthenium catalyst (Equation 1.3).[4] This process yields millions of tons of ammonia annually, and fertilizer that is made from this ammonia is responsible for sustaining approximately 40% of the world's

population.[38] Two Nobel Prizes were given for the discovery of the Haber-Bosch Process: the first was awarded to Fritz Haber in 1918, for discovering the nitrogen fixation reaction, and the second was awarded to Carl Bosch in 1931, for developing the high-pressure techniques that made this process industrially feasible.

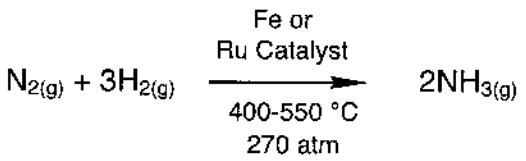

Equation 1.3

1.3 The Chemistry of Side-on End-on Dinitrogen.

This thesis will focus on the chemistry of the side-on end-on N_2 complex $([NPN]Ta)_2(\mu\text{-}H)_2(\mu\text{-}\eta^1{:}\eta^2\text{-}N_2)$ (where [NPN] = $[(PhNSiMe_2CH_2)_2PPh]^{2-}$), which will be noted as **1** below.[39] Complex **1** contains two tridentate [NPN] ligands that are each bound to two formally Ta(V) metal centers.

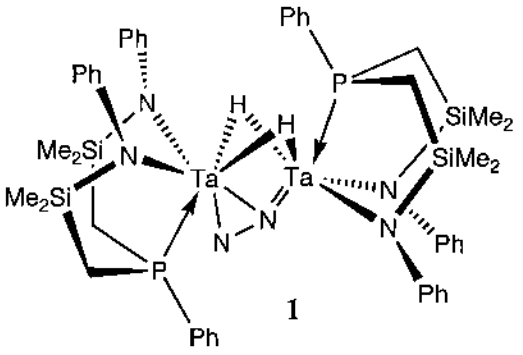

1

The two Ta(V) centers are also bound η^1-η^2 to the nitrogen molecule. The ligand synthesis is outlined in Scheme 1.1.[39] The reaction of 2 equivalents of $ClCH_2SiMe_2NHPh$ with 4

equivalents of *n*-BuLi and 1 equivalent of $PhPH_2$ produces Li_2[NPN], which in turn reacts with Me_3TaCl_2 to form [NPN]$TaMe_3$ via a metathesis reaction.

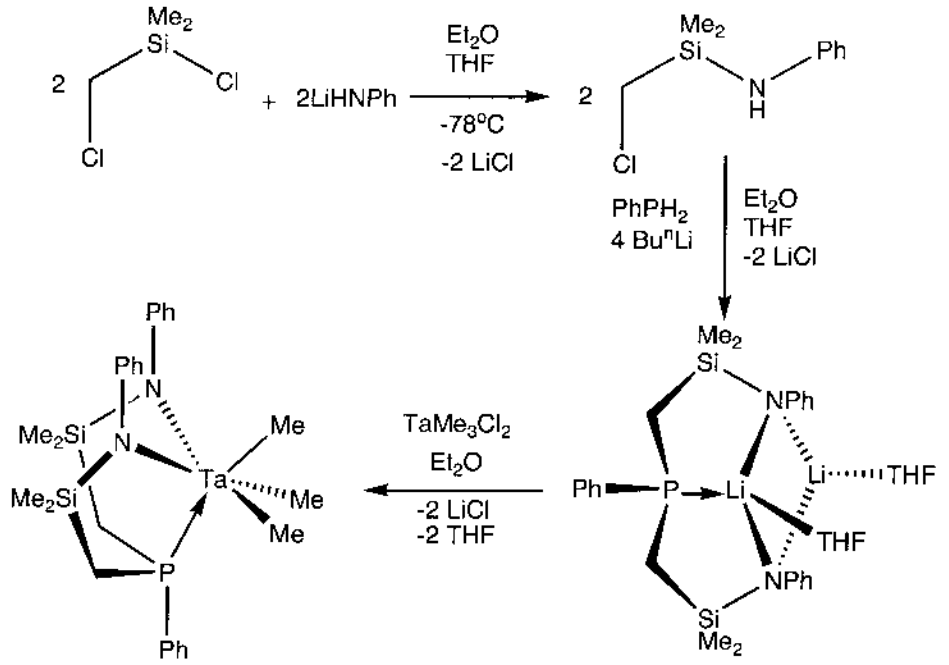

Scheme 1.1

Upon exposure of [NPN]$TaMe_3$ to 4 atm of H_2, the purple, diamagnetic Ta(IV)-Ta(IV) complex, ([NPN]Ta)$_2$(μ-H)$_4$, **2**, is produced (Equation 1.4). An ORTEP depiction of the solid-state molecular structure of this tetrahydride complex, along with selected bond lengths and bond angles is shown in Figure 1.3.

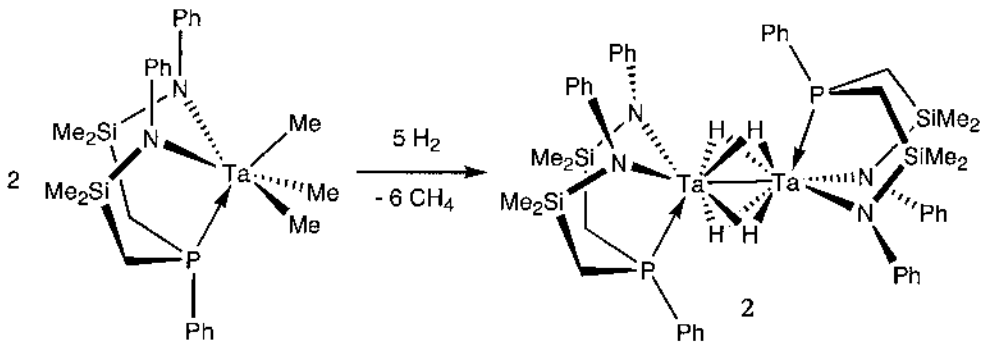

Equation 1.4

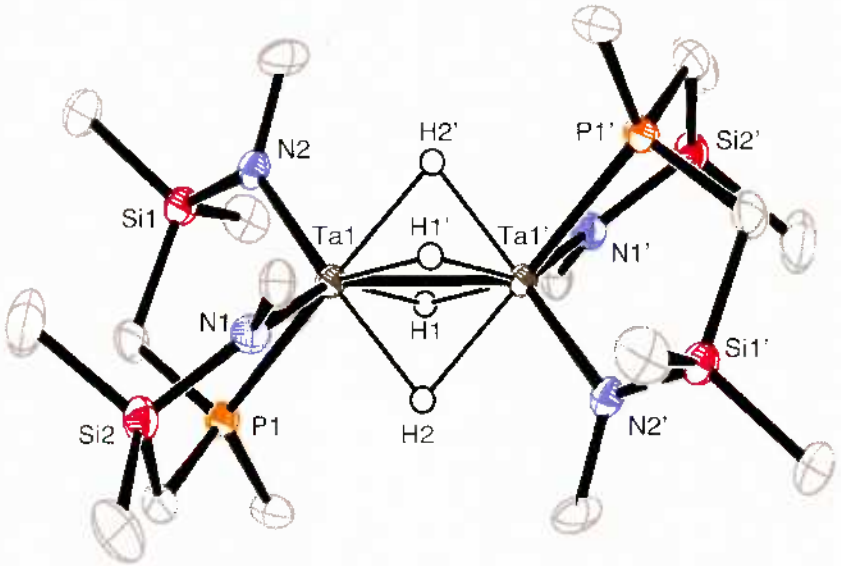

Figure 1.3 ORTEP depiction of the solid state molecular structure of ([NPN]Ta)$_2$(μ-H)$_4$, **2** (ellipsoids at 50% probability). Hydrides were located on a difference map and refined isotropically, and tantalum hydride bond lengths were determined by PARST. All hydrogen atoms and phenyl ring carbons other than *ipso* carbons have been omitted for clarity. Selected bond lengths (Å) and bond angles (°): Ta1-Ta1' 2.5602(8), Ta1-H1 1.8471(290), Ta1-H2 1.8542(258), Ta1-N1 2.093(2), Ta1-N2 2.058(2), Ta1-P1 2.5741(10), H1-Ta1-H2 59.98(4), N1-Ta1-H1 90.81(8), N1-Ta1-H2 148.27(4), N2-Ta1-H1 155.17(1), N2-Ta1-H2 96.03(7), P1-Ta1-H1 86.65(7), P1-Ta1-H2 83.45(8) N1-Ta1-N2 110.69(10), N1-Ta1-Ta1' 119.66(7), N2-Ta1-Ta1' 123.26(7), N1-Ta1-P1 82.65(7), N2-Ta1-P1 84.08(8), P1-Ta1-Ta1' 125.06(3).

The solid-state structure of **2** is C_i symmetric, and the ^{1}H and ^{31}P{^{1}H} NMR spectra[10] indicate that **2** is also C_i symmetric in solution; this is in contrast to that observed

for **1**, which is C_s symmetric in solution. Selected bond lengths for **1** and **2** are shown in Table **1.3**.

Table 1.3. A comparison of selected bond lengths (Å) for **1** and **2**.

([NPN]Ta)$_2$(μ-H)$_4$, **2**			([NPN]Ta(μ-H))$_2$({μ-η^1:η^2-N$_2$}), **1**		
Atom	**Atom**	**Distance (Å)**	**Atom**	**Atom**	**Distance (Å)**
Ta1	Ta2	2.5602(8)	Ta1	Ta2	2.8311(3)
Ta1	N1	2.093(2)	Ta1	N1	2.066(5)
Ta1	N2	2.058(3)	Ta1	N2	2.040(5)
Ta1	P1	2.5741(10)	Ta1	P1	2.625(2)

The Ta1-Ta1' bond length in **2** is 2.5602(8) Å, which is considerably shorter than the Ta1-Ta2 separation for **1** (2.8311(3) Å). A slightly smaller difference is observed with the Ta-N and Ta-P bonds. The Ta1-N1 and Ta1-N2 bond lengths for **2** (2.093(2) and 2.058(2) Å, respectively) are slightly longer than that of **1** (Ta1-N1 = 2.066(5), Ta1-N2 = 2.040(5)), and the Ta1-P1 for **2** (2.5741(10) Å) is slightly shorter than that for **1** (Ta1-P1 = 2.625(2) Å).

([NPN]Ta)$_2$(μ-H)$_4$ reacts with N_2 gas to form **1**, (N-N bond: 1.319(4) Å), as shown in Equation 1.5. The yield of the reaction is improved if a mixture of 90% N_2 and 10% H_2 gases are used, although the precise mechanism of this is unknown.[40]

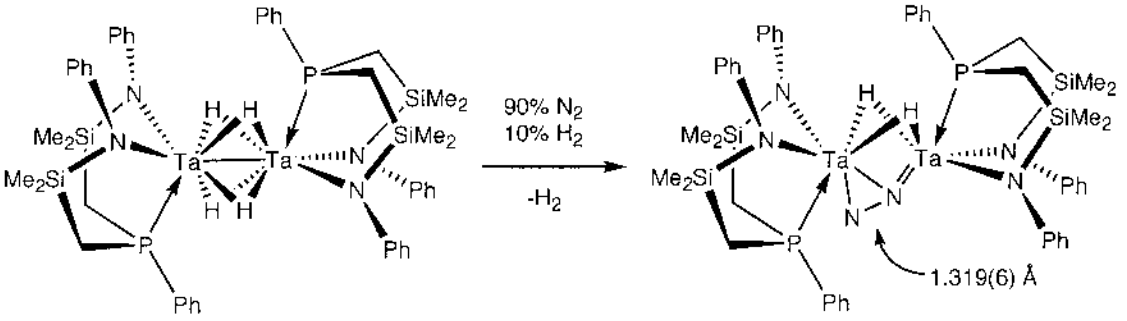

2 **1**

Equation 1.5

The formation of **1** from **2** is interesting for many reasons. Firstly, the use of alkali metal reducing agents, (such as Na and KC_8), which are commonly used to form dinitrogen complexes, are avoided. Secondly, this is a rare example of forming an activated early transition metal dinitrogen complex by displacing H_2,[41,42] although this reaction is known for late transition metals.[43,44]

Complex **1** is also impressive in its wide scale of reactivity. In some cases, the side-on end-on N_2 can act as a nucleophile (Equation 1.6); for instance, **1** reacts with benzyl bromide to give the *N*-benzyl derivative, {[NPN]Ta(Br)}$_2$(μ-H){μ-η^1-η^2-NN(CH$_2$-C$_6$H$_5$)}(Ta[NPN]), **3**, (N-N bond: 1.353(4) Å).[40]

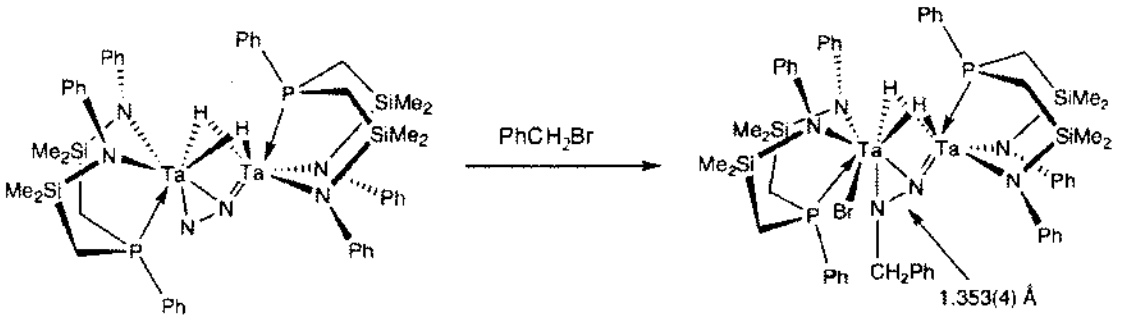

Equation 1.6 **3**

The reaction of **1** with simple hydride reagents E-H (E-H = 9-BBN (HBR_2), DIBAL ($HAlR_2$) and H_3SiBu^n) results in the functionalization of N_2.[45-47] The first step is formation **4** via E-H addition across the Ta-N bond (Scheme 1.3). Complex **4** has been characterized in the solid-state for E = BR_2 or SiH_2Bu^n, and in solution by NMR spectroscopy for E = $AlBu^i_2$.[45-47] Second, H_2 elimination and cleavage of the N-N bond is common to these processes to form intermediate **5**, (Scheme 1.2).

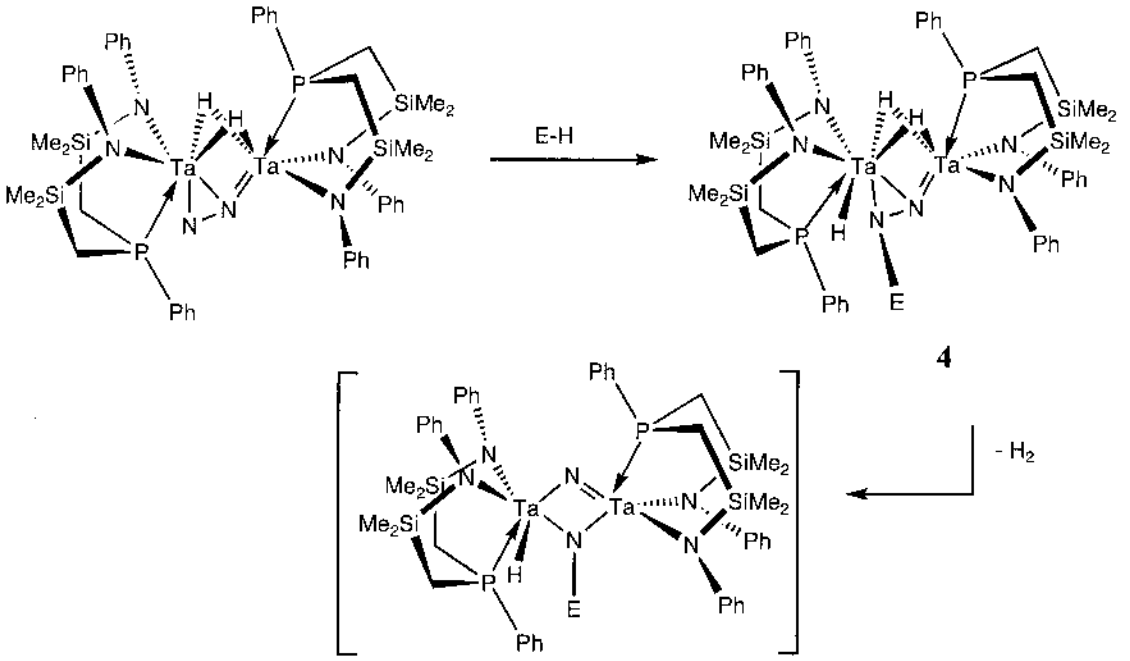

Scheme 1.2

Intermediate **5** will yield different products depending on the hydride source (Scheme 1.3). Hydroboration of **1** (where E = BC_8H_{14}) degrades the [NPN] ligand and eliminates H_2 from the bridging hydrides to form to form [(PhNSiMe$_2$CH$_2$P(Ph)CH$_2$-SiMe$_2$μ-N)Ta(=NBC$_8$H$_{14}$)](μ-N)(Ta[NPN]), **6**, along with one equivalent of benzene from the N-Ph of [NPN]. In this process, N_2 is cleaved and functionalized.[45]

Hydroalumination of **1** (where E = Al^{i}Bu$_2$) produces ([NPN]TaH)(μ-H)(μ-η^1:η^2-N$_2$Al(μ-H)^{i}Bu)(Ta[NPN]), **7**.[46] In this process, one equivalent of isobutene is eliminated, and N_2 is cleaved and functionalized; however, although ligand degradation is not observed, one amide donor of [NPN] migrates from Ta to Al.

Hydrosilylation of **1** produces ([NPN]Ta)$_2$(μ-NSiH$_2$Bu^n)$_2$, **8**, a symmetrical disilylimide complex that has a cleaved and functionalized N_2; in this complex, [NPN] remains intact.[47]

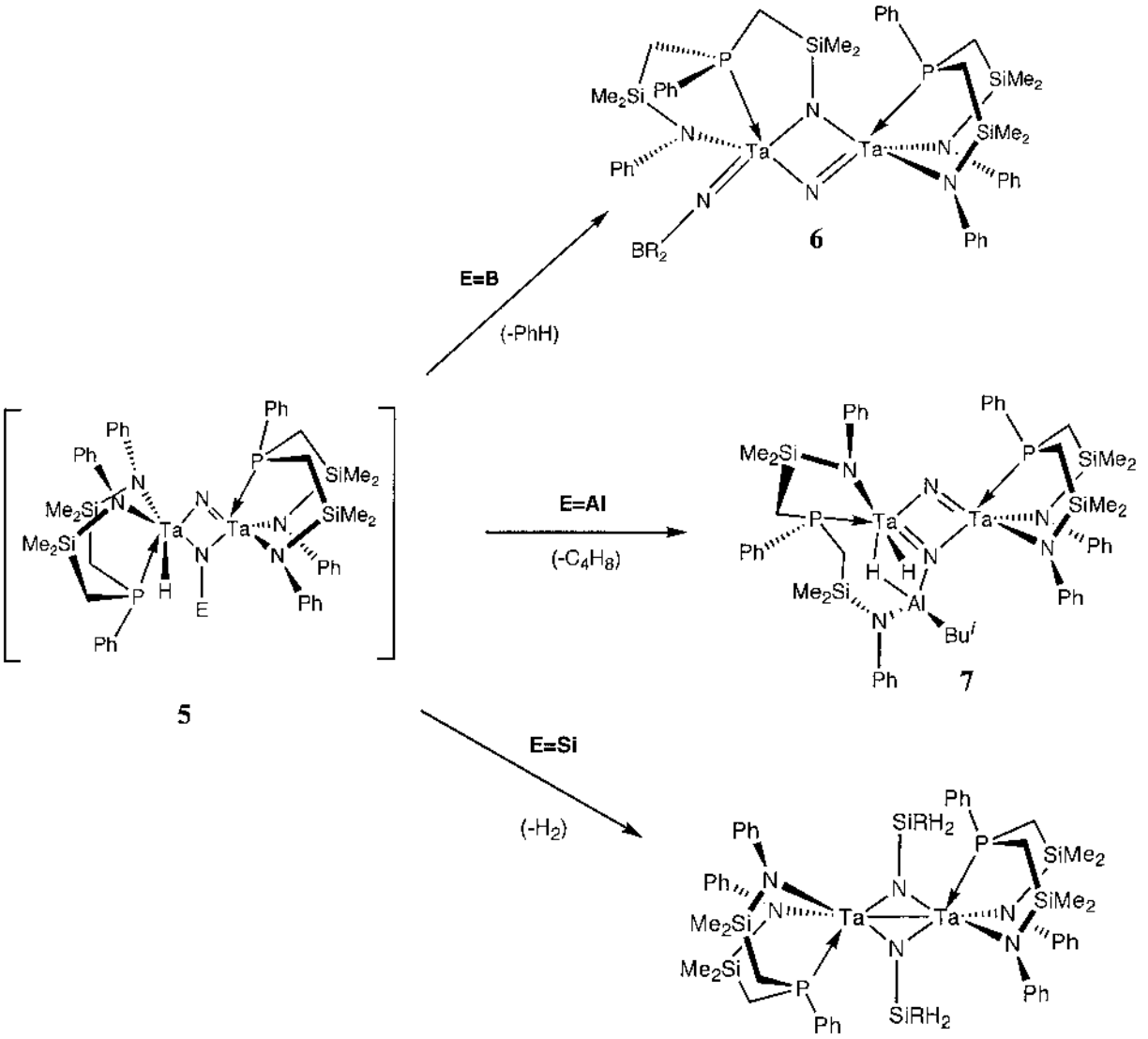

Scheme 1.3

1.4 Scope and Prospectus.

The central goal of this thesis is to explore new types of reactivity that lead to the cleavage and functionalization of N_2 in ([NPN]Ta(μ-H))$_2$(μ-η^1:η^2-N_2), **1**. In Chapter Two, the reactivity of **1** with several alkene reagents is investigated. Migratory insertion with primary alkenes occurs to form an activated end-on N_2 alkyl complex. The synthesis and characterization of these complexes is discussed.

The focus of Chapter Three is the reactivity of **1** with group IV and V metallocenes. With group IV metallocenes, N_2 is cleaved and functionalized. In contrast, group V metallocenes did not react with **1**, and the reasons for this will be explained in this chapter.

In Chapter Four, the reactivity of **1** with GaCp* forms a new complex, **18**, that was characterized using NMR spectroscopy. Complex **18** decomposes into a number of different P-containing species over the course of several days, as evident in the $^{31}P\{^1H\}$ NMR spectrum. One of these species, **19**, was isolated and characterized using X-ray diffraction. The solid-state structure showed evidence of ligand rearrangement, a process that was previously observed with hydroboration reactions of **1**. The mechanism and characterization of **18** will be discussed in this chapter, along with a general summary of this thesis, and some suggested future work.

Chapter Two

Olefin Insertion Reactions of the Side-on End-on Dinitrogen Complex

2.1 Introduction.

Olefin insertion of M-H bonds is an important elementary step in many catalytic reactions.[48] In its simplest terms, an olefin-hydride insertion is the addition of a metal-hydride bond across the π bond of an unsaturated hydrocarbon.[49] This addition is a concerted process that occurs via the formation of a four-centered transition state (Figure 2.1).[50]

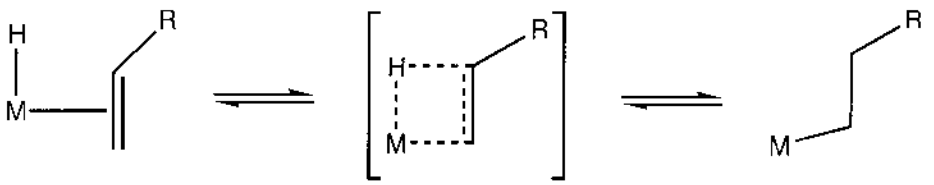

Figure 2.1. An illustration of the four-centered transition state formed in an olefin-hydride insertion.

Molecular orbital studies have contributed to a better understanding of this process.[51-54] These studies describe the key orbital interactions involved in olefin-hydride insertion; first, the alkene π orbital donates electrons to the LUMO antibonding σ^*_{MH} orbital; second, back donation from the HOMO σ_{MH} orbital to the olefin π^* orbital creates a cyclic transition state that activates the insertion of the olefin into the metal hydride, to generate an alkyl transition-metal complex.

For a concerted reaction, the activation energy is typically lower than the bond dissociation energies of the weakest bonds to be broken.[50] Some examples of hydride complexes and the activation energies for insertion of ethylene are provided in Figure 2.2.[55-59] An explanation of the factors that affect the energy barrier for hydride-olefin insertion is beyond the scope of this chapter; however, the repulsion between non-bonding metal electrons and the electrons in the olefin, the type of ligands and metals that are used, and the electronic state of the olefin, have all shown to be factors in the activation barrier.[48,55,57,58]

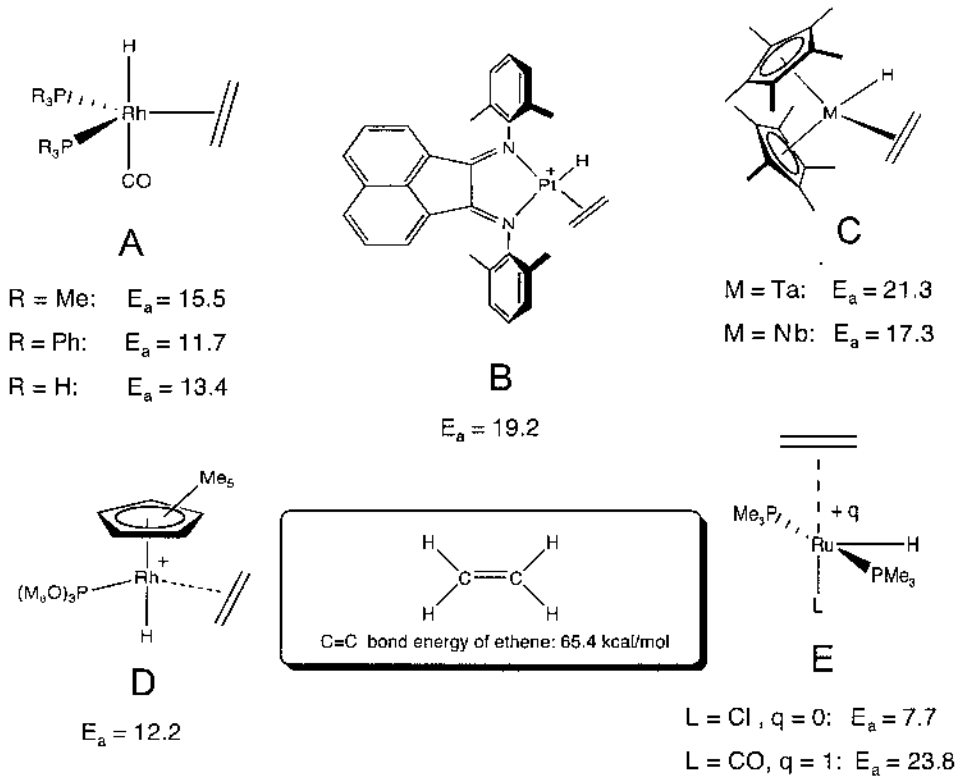

Figure 2.2. Examples of hydride-olefin complexes and the activation energies (kcal/mol) associated with the hydride-insertion into ethylene. For comparison, the C=C bond energy for ethylene is shown in the inset.

The orientation of the olefin relative to the M-H bond is also important for the concerted reaction. The olefin must coordinate *cis* to the M-H bond in order to form a coplanar M-C-C-H fragment upon reaction (see Figure 2.3).[49] Although **A** and **B** in Figure 2.3 both have a cis arrangement of the alkene and the M-H bond, **A** undergoes insertion at least 40 times faster than **B** because the M-C-C-H moiety can be coplanar.[60]

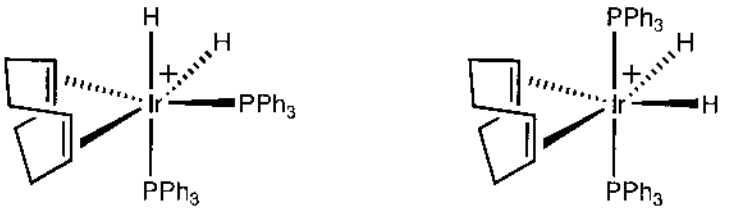

A **B**

Figure 2.3. Two complexes in which the hydride and olefin ligands are cis. Complex **A** undergoes insertion faster than **B**.

2.2 Olefin Insertion Reactions.

Olefin-insertion is a crucial step in many reactions, and is commonly explored with terminal transition metal-hydrides. There are only a few reported cases of olefin insertion into bridging transition metal-hydrides, some of which will be discussed in section 2.2.1. Hydrozirconation also features an olefin-hydride insertion to generate new organic products; this process, along with the reaction of **1** with propene, will be described in sections 2.2.2, and 2.2.3, respectively.

2.2.1. Olefin Insertion Reactions of Bridging Hydride Complexes.

The few reported cases of olefin-insertion reactions with bridging-hydride complexes have been limited to group 3 metal-hydrides.[61-63] A kinetic study with $(Cp^*_2YH)_2$ revealed that this process can occur via an associative or dissociative mechanism (Scheme 2.1).[63] The associative mechanism involves the attack of the olefin on the metal-hydride, to generate two intermediates: an olefin-coordinated intermediate that undergoes insertion, and a second mono-hydride intermediate, which binds to an olefin and undergoes insertion. In the dissociative mechanism, the bridged-hydride complex forms two mono-hydride intermediates, and then coordinates an olefin, which undergoes insertion. Both processes depend on several factors, including the rate of dissociation of the hydride-dimer, the steric environment of the olefin, and of the metal-alkyl complex. For instance, the reaction of $(Cp^*_2YH)_2$ with unhindered olefins, such as propene, butene and hexene, forms mono- or double- inserted products through an associative process. On the other hand, the reaction of $(Cp^*_2YH)_2$ with sterically hindered olefins, such as 3-methyl butene, 2-methyl propene, occurs through a dissociative process and only forms mono-inserted products.

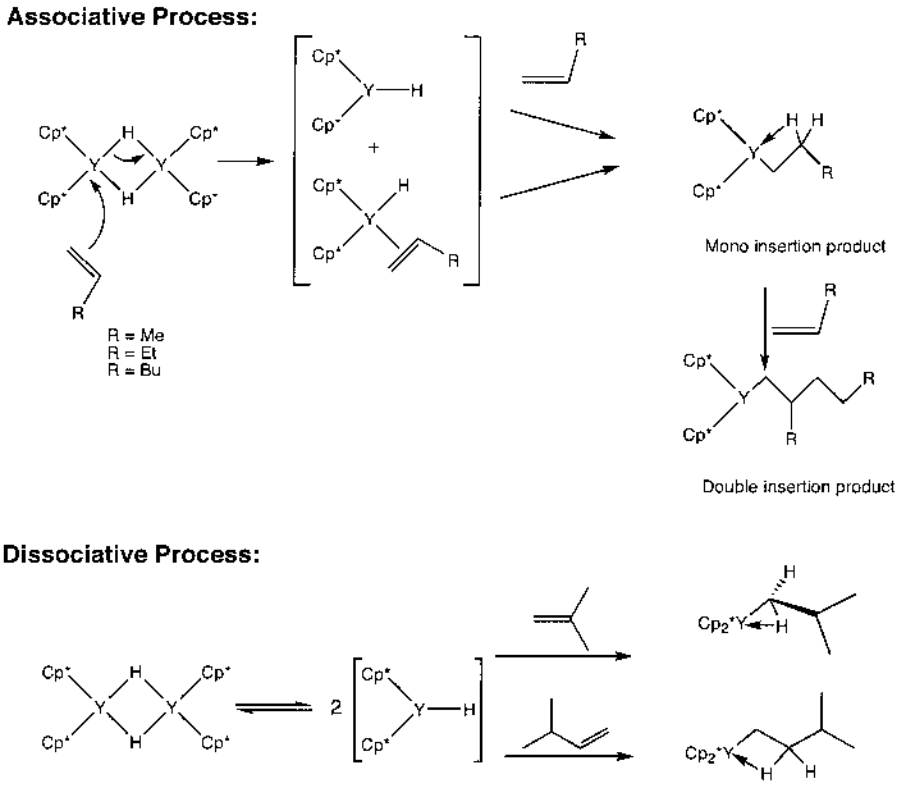

Scheme 2.1.

In some instances, olefin-insertion with group 3 bridged-hydride complexes can form bridging-alkyl complexes. For example, yttrium and scandium (Scheme 2.2) hydride dimers can react with primary olefins to form η^1-and η^2- alkyl-bridged complexes.[61,62]

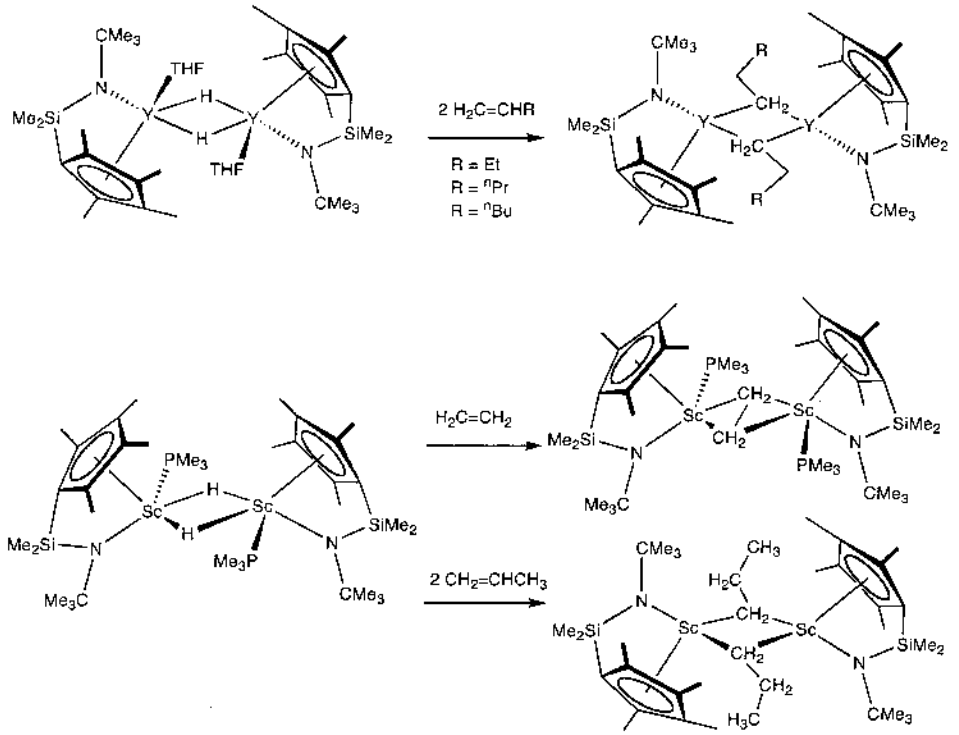

Scheme 2.2.

2.2.2. Hydrozirconation of Olefins.

Hydrozirconation is the reaction of Cp_2ZrHCl (Schwartz's reagent) and an unactivated* alkene to generate the alkylzirconium(IV) product, $Cp_2Zr(R)Cl$.[64] This process involves either the regiospecific addition of Zr-H to a terminal double bond, or Zr-H addition to an internal double bond, followed by rearrangement via Zr-H elimination and readdition to place the metal at the least hindered position of the alkyl chain. Subsequent reactions of $Cp_2Zr(R)Cl$ produce a wide range of organic compounds, depending on the reagent that is used. For example, electrophilic halogenation reagents, such as Br_2, I_2, *N*-bromo- (NBS) or *N*-chloro-succinimide (NCS), to $Cp_2Zr(R)Cl$ affords organic halides (RX)

* The term 'unactivated' refers to olefins that are substituted with alkyl or proton substituents only.

and $Cp_2Zr(X)Cl$.[65,66] The reaction of $Cp_2Zr(R)Cl$ with oxidizing reagents such as basic hydrogen peroxide, *tert*-butyl hydroperoxide, and *m*-chloro-perbenzoic acid yields alcohols.[67] $Cp_2Zr(R)Cl$ undergoes an insertion reaction with carbon monoxide to yield an acylzirconium(IV) species that reacts subsequently with acids, Br_2/CH_3OH, hydrogen peroxide and NBS to generate aldehydes, esters, carboxylic acids, and acyl halides, respectively.[68] These reactions are illustrated in Figure 2.4.

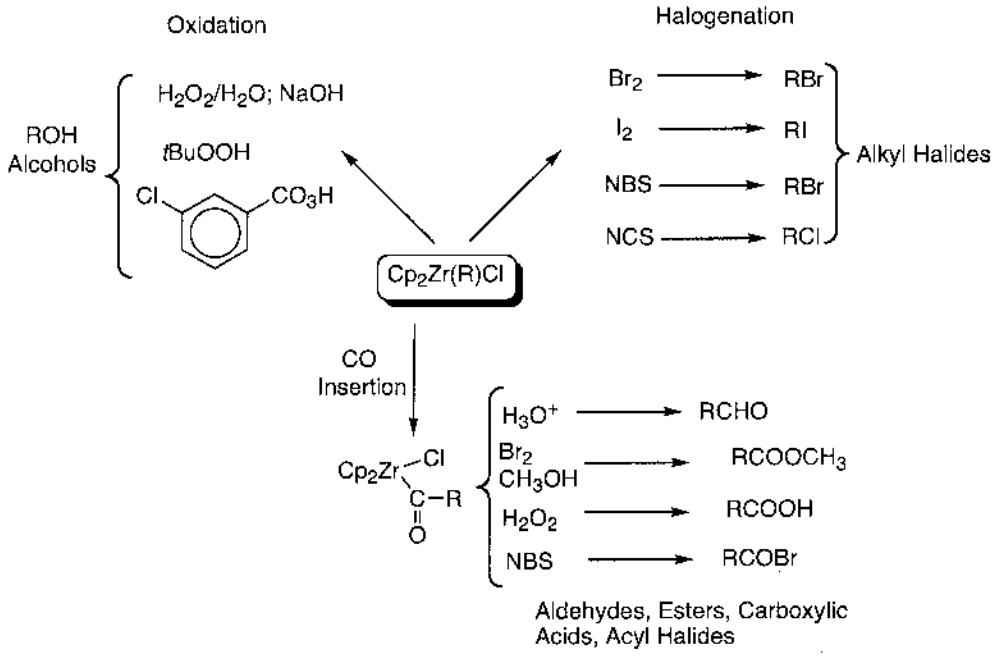

Figure 2.4. Subsequent reactions of $Cp_2Zr(R)Cl$.

2.2.3. Olefin Insertion with ([NPN]Ta(μ-H)$_2$(μ-η^1:η^1-N$_2$).

The formation of dark red ([NPN]Ta(CH$_2$)$_2$CH$_3$)$_2$(μ-η^1:η^1-N$_2$), **9**, from **1** and propene over two weeks in toluene was described in 2001 (Equation 2.1).[69] In **9**, N_2 bridges the two tantalums end-on, and is moderately activated (N-N bond: 1.289(6) Å). This was the first report of olefin insertion via hydride migration using **1**.

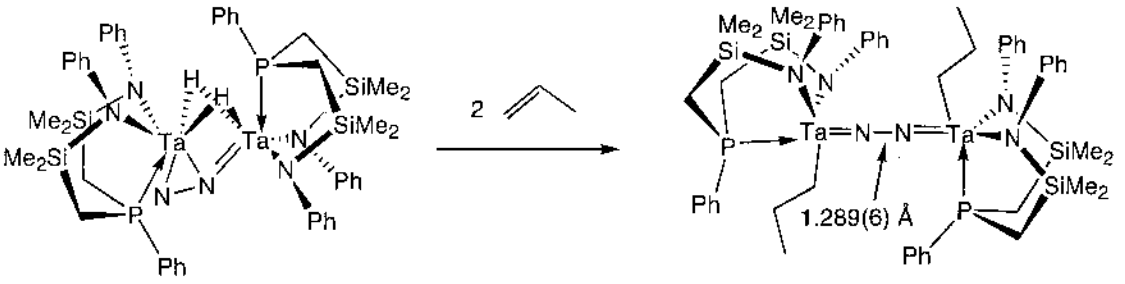

1 **9**

Equation 2.1

It is likely that the bridging hydrides in **1** force N_2 into the side-on end-on configuration. Thus, the hydride migration reaction of **1** with olefins is likely to provide products in which the bonding mode of N_2 has been transformed, and the extension of this reaction to other alkenes is of interest. The reaction of **1** with 1-pentene and 1-hexene was investigated to see if it would affect the activation of coordinated dinitrogen in **1**.

2.3 Results and Discussion.

2.3.1. Reaction of 1 with 1-pentene.

Given that hydride migration was observed with propene for the formation of **9**, a similar reaction was attempted with 1-pentene. Stirring a brown mixture of 1-pentene and **1** in benzene overnight at 65°C generated a yellow-red solution, from which red ([NPN]Ta $(CH_2)_4CH_3)_2(\mu\text{-}\eta^1\text{:}\eta^1\text{-}N_2)$, **10**, was isolated in 82% yield (Equation 2.2).

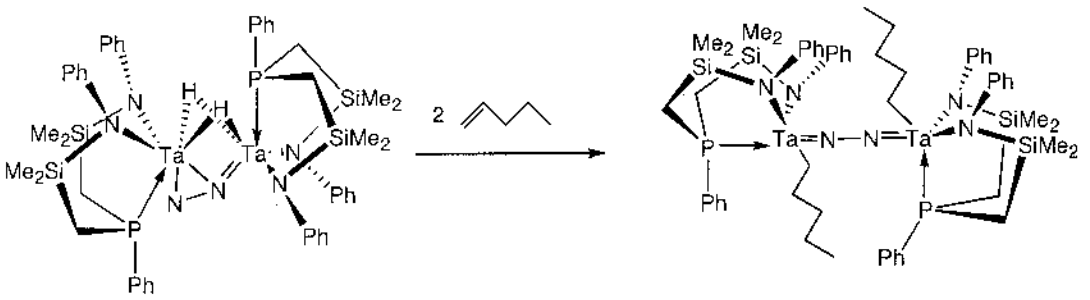

1 **10**

Equation 2.2

The $^{31}P\{^1H\}$ NMR spectrum of **10** reveals two singlets at δ 4.69 and 20.0 (Figure 2.5), which indicate two different ^{31}P environments. The ^1H NMR spectrum of **10** is C_s symmetric, with inequivalent pentyl and silyl methyl resonances (Figure 2.6). The presence of two different ligand and alkyl environments was determined using ^1H-COSY and ^1H, ^{13}C-HSQC spectroscopy. The absence of a peak attributable to a bridging or terminal hydride and the presence of alkyl ligand resonances in the ^1H NMR spectrum, indicate that olefin insertion into the metal hydride has occurred in the formation of **10**.

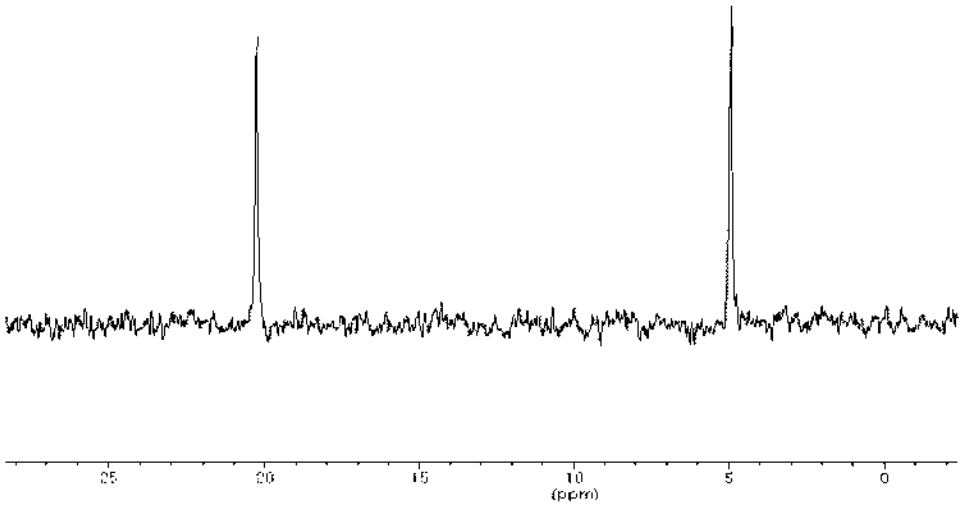

Figure 2.5. $^{31}P\{^{1}H\}$ NMR spectrum of **10** in C_6D_6.

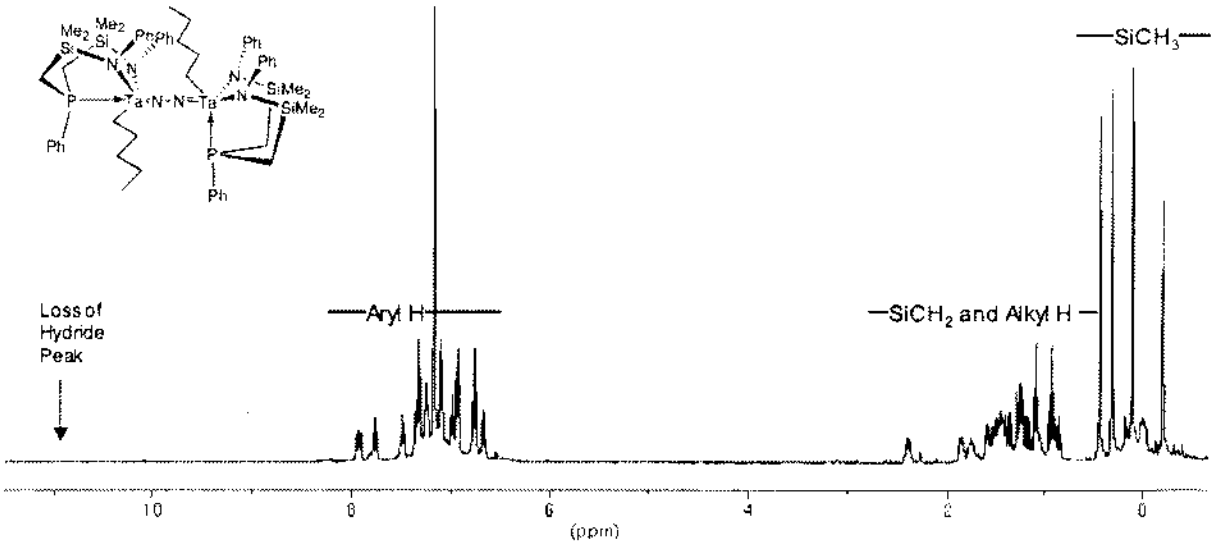

Figure 2.6. 300 MHz ^{1}H NMR spectrum of **10** in C_6D_6.

The $^{15}N_2$ labeled species ([NPN]Ta$(CH_2)_4CH_3)_2(\mu\text{-}\eta^1\text{:}\eta^1\text{-}^{15}N_2)$, **10-$^{15}N_2$,** was prepared from the reaction of **1-$^{15}N_2$** and 1-pentene. The $^{31}P\{^1H\}$ NMR spectrum of **10-$^{15}N_2$** shows two resonances, a singlet at δ 20.0, and a resonance at δ 4.69 coupled to two different $^{15}N_2$ environments, with coupling constants of 30.5 and 6.5 Hz (Figure 2.7).

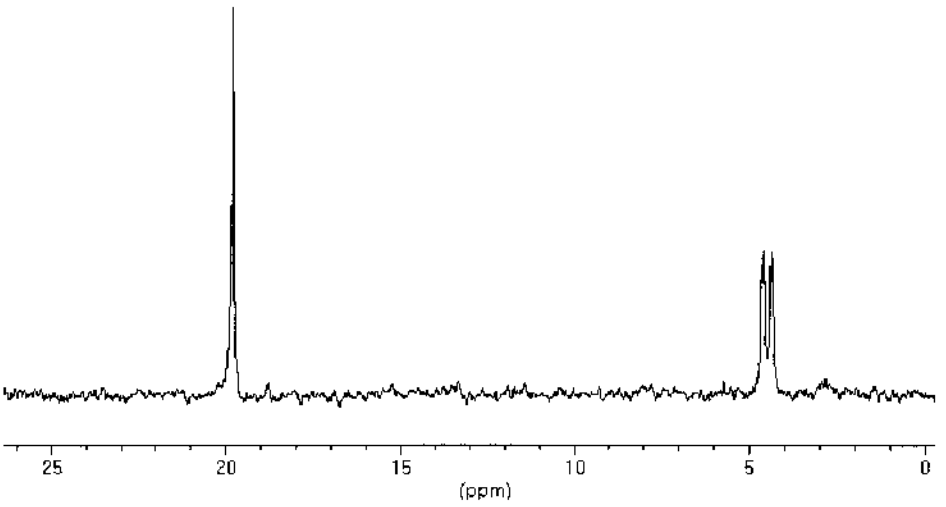

Figure 2.7 $^{13}P\{^1H\}$ NMR spectrum of **10-$^{15}N_2$** in C_6D_6.

The $^{15}N\{^1H\}$ NMR spectrum of **10-$^{15}N_2$** has two doublets of doublets at δ 14.1 and 25.9 (Figure 2.8). The resonance at δ 14.1 is coupled to one ^{15}N with a $^1J_{NN}$ value of 11.5 Hz, and also to one ^{31}P with $^2J_{PN}$ = 30.5 Hz. The second resonance at δ 25.9 exhibits the same one-bond coupling to ^{15}N where $^1J_{NN}$ = 11.5 Hz, and a three-bond coupling to ^{31}P with a coupling constant of 6.5 Hz. The coupling constants are similar to those observed in the $^{15}N\{^1H\}$ NMR spectrum of **9**: $^1J_{NN}$ = 11.3 Hz, and a two- and three-bond N-P coupling at 30.5 and 6.6 Hz respectively. X-ray quality crystals could not be obtained for **10**, but the

NMR data suggests that in solution, **10** is C_s symmetric and has two chemically different tantalum centers, like **9**.

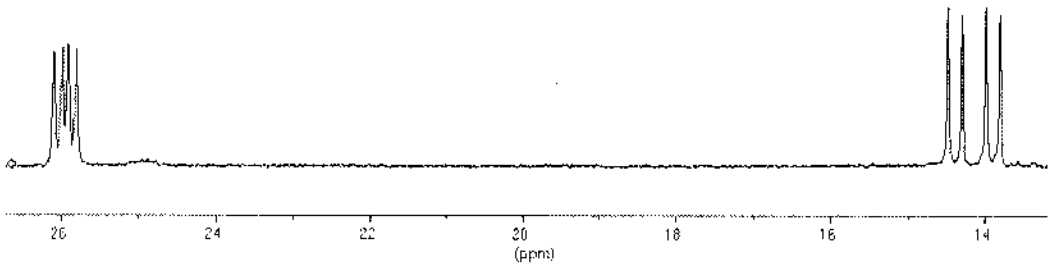

Figure 2.8. $^{15}N\{^1H\}$ NMR spectrum of **10** in C_6D_6.

2.3.2. Reaction of 1 with 1-hexene.

Complex ([NPN]Ta$(CH_2)_5CH_3)_2(\mu\text{-}\eta^1\text{:}\eta^1\text{-}N_2)$, **11**, was prepared in the same manner as **10**, except 1-hexene was used instead of 1-pentene. Upon heating the mixture, the solution changed from brown to dark red, and a red precipitate ([NPN]Ta$(CH_2)_5$-$CH_3)_2(\mu\text{-}\eta^1\text{:}\eta^1\text{-}N_2)$, **11**, was collected in 86% yield (Equation 2.3).

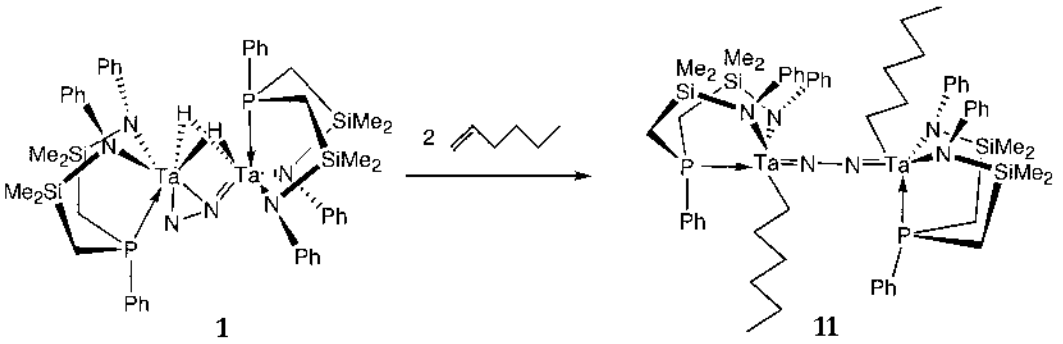

Equation 2.3

^{1}H NMR spectroscopy, in conjunction with ^{1}H-COSY and ^{1}H, ^{13}C-HSQC spectroscopy, showed the absence of upfield resonances attributable to hydride ligands, and the presence of two chemically inequivalent ligand and alkyl environments. The ^{31}P{^{1}H} NMR spectrum of **11** in C_6D_6 shows two singlets δ 6.46 and 21.75. The ^{1}H NMR spectra of **11** shows four inequivalent silyl methyl resonances, and two chemically different ligand and alkyl environments. ([NPN]Ta$(CH_2)_5CH_3)_2(\mu\text{-}\eta^1\text{:}\eta^1\text{-}^{15}N_2)$, **11-^{15}N$_2$** was also prepared, and the ^{31}P{^{1}H} NMR spectrum of **11-^{15}N$_2$** shows two resonances - a singlet at δ 22.0, and a doublet of doublets δ 6.93 with $^2J_{PN}$ = 29.5 Hz, and $^3J_{PN}$ = 6.5 Hz. ^{15}N NMR spectroscopy for **11** showed two doublets of doublets at δ 14.15 and 25.94 (Figure 2.9). The resonance at δ 14.15 has a one-bond ^{15}N coupling of $^1J_{NN}$ = 11.3 Hz, and a two-bond coupling to ^{31}P at $^2J_{PN}$ = 29.5 Hz. The peak at δ 25.94 showed the identical one-bond coupling to ^{15}N of $^1J_{NN}$ = 11.3 Hz, and a three-bond coupling to ^{31}P of 6.5 Hz. X-ray quality crystals were formed from benzene by slow evaporation, and the solid state molecular structure of **11** was determined by X-ray diffraction. An ORTEP depiction of **11** with selected bond lengths and bond angles is shown in Figure 2.10.

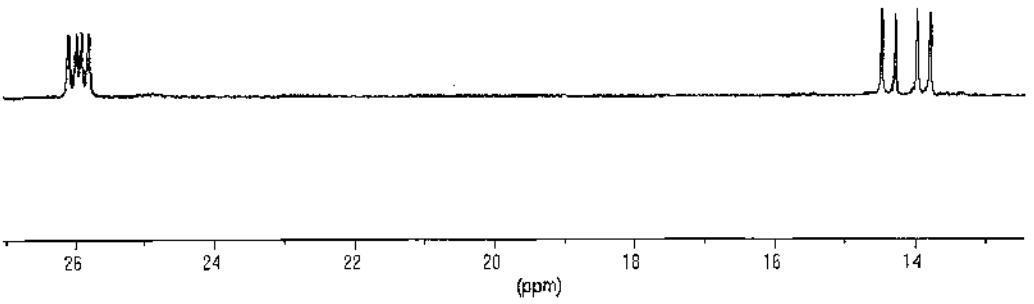

Figure 2.9. ^{15}N{^{1}H} NMR spectrum of **11** in C_6D_6.

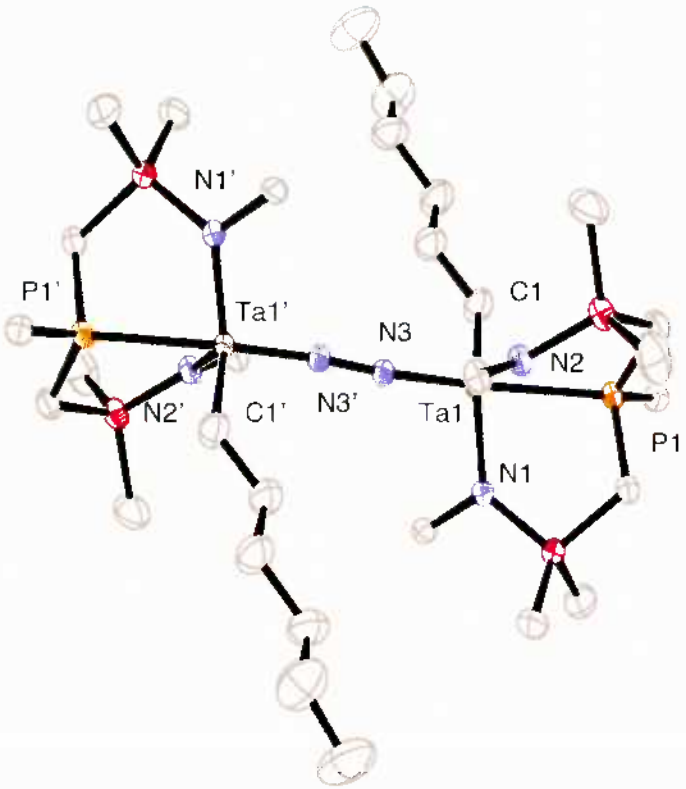

Figure 2.10. ORTEP depiction of the solid state molecular structure **11**, (ellipsoids at 50% probability). All hydrogen atoms and phenyl ring carbons other than *ipso* carbons have been omitted for clarity. Selected bond lengths (Å) and bond angles (°): Ta1-N1 2.043(3), Ta1-N2 2.042(3), Ta1-N3 1.820(3), Ta1-C1 2.200(4), Ta1-P1 2.6851(10), N3-N3' 1.272(6), N1-Ta1-N2 115.42(13), N1-Ta1-N3 100.06(14), N2-Ta1-N3 104.37(13), N1-Ta1-P1 75.50(9), N1-Ta1-C1 121.68(17), C1-Ta1-N2 113.94(17), C1-Ta1-N3 95.95(16), P1-Ta1-N3 175.20(10), P1-Ta1-N2 79.41(9), C1-Ta1-P1 85.05(12).

The solid-state structure of **11** has an N-N bond distance of 1.272(6) Å, which is similar to the N-N bond length found in **9** (N-N = 1.289(6) Å). The stereochemistry about the tantalum metal is distorted triganol bipyramidal, where atoms P1 and N3 occupy the

axial positions, and atoms C1, N1 and N2 occupy the equatorial. In contrast to its C_s symmetry in solution (C_6D_6, rt), the solid-state structure of **11** is C_i symmetric. A possible explanation for this anomaly is that **11** exists as an equilibrium (see Equation 2.4) between the predominant *cis-trans* isomer (**11A**) at room temperature, and the minor *trans-trans* isomer (**11B**).

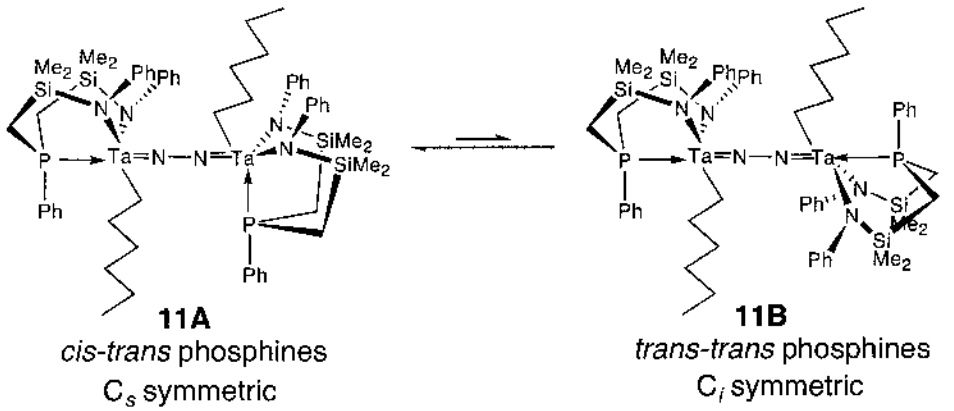

Equation 2.4

The possibility that the equilibrium in Equation 2.4 could occur suggested that a $^{31}P\{^1H\}$ VT-NMR study would be informative for this process. Figure 2.11 shows a low-temperature stack-plot of $^{31}P\{^1H\}$ spectra of **11** in toluene acquired every 30 minutes with 10 K degree intervals, from 273 K (bottom) to 203 K (top). Integration of the peaks in Figure 2.11 with respect to temperature (K) shows an inverse relationship between **11A** (δ 6.46 and δ 21.75) and **11B** (δ 4.96); at lower temperatures, the resonance for **11B** (δ 4.96, purple) begins to emerge, and the resonances at δ 21.75 (green) and δ 6.46 (pink) assigned to the *cis-* and *trans-* phosphorus atoms of **11A** respectively, begin to decrease. The new resonance at δ 4.96 is a singlet (consistent with a symmetric phosphine complex) and close

in range to the *trans*-phosphorus resonance of **11A** at δ 6.46, supporting the formation of **11B**.

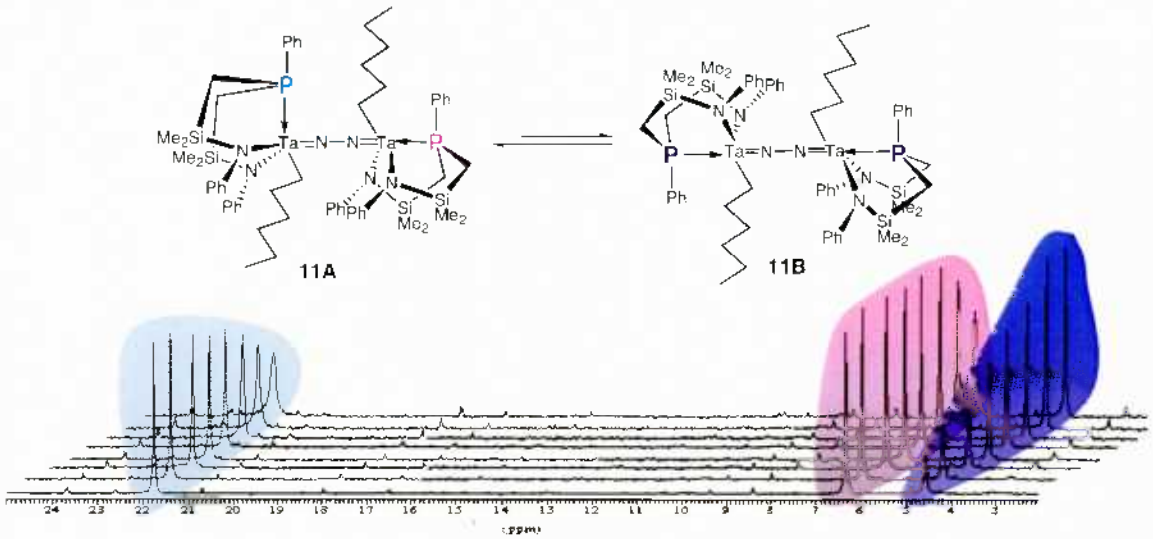

Figure 2.11. $^{31}P\{^{1}H\}$ spectra of **11** in toluene from 273 K (bottom) to 203 K (top) in -10 K increments.

A Van't Hoff graph of $\ln(K_{eq})$ vs $1/T$ (K^{-1}) shows the correlation of K_{eq} as a function of temperature (Figure 2.12). K_{eq} was taken at each temperature as the integral of **11B** divided by the average integral of **11A**, according to Equation 2.5 (below). The graph shows a positive linear correlation in the formation of **11B** with decreasing temperature.

K_{eq} = Integration of **11B** (T)/ Average Integration of **11A** (T)

Equation 2.5

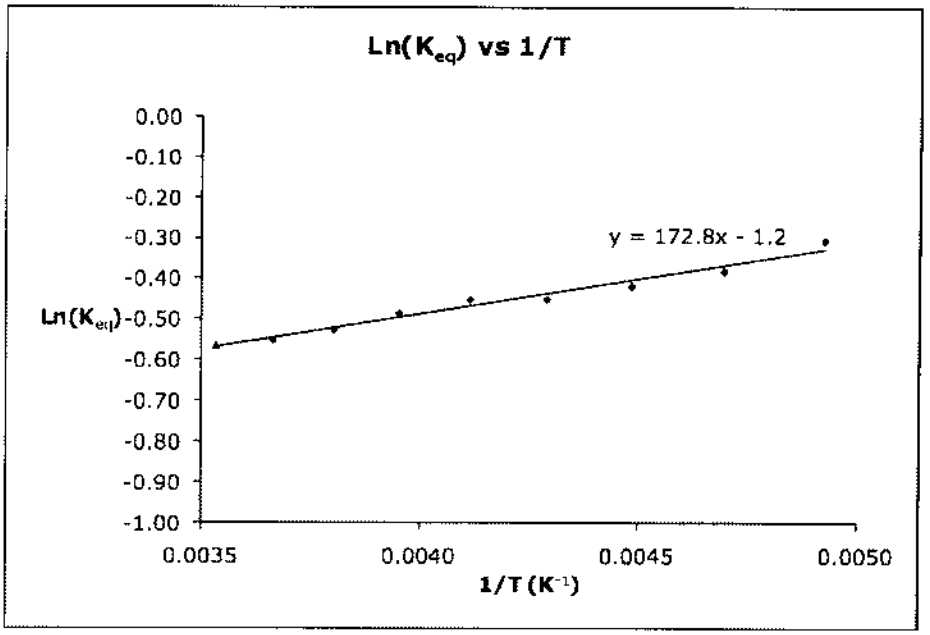

Figure 2.12 A Van't Hoff plot, $\ln(K_{eq})$ vs 1/T from 283 K to 203 K.

From the Van't Hoff plot of $\ln(K_{eq})$ vs 1/T (Figure 2.12), the enthalpy ($\Delta H°$) and entropy ($\Delta S°$) were determined using the slope of the line and the y-intercept (Equation 2.6 and Equation 2.7). The thermodynamic parameters for the equilibrium are $\Delta H°$ = -1.4 kJ/mol and $\Delta S°$ = -9.8 J/K, which are relatively small and consistent with an equilibrium between two very similar species. Although the data supports the existence of an equilibrium, the reason as to why **11B** is preferred over **11A** in the solid-state is unknown, and it is presumed that packing effects of the alkyl groups in the crystal favour the C_i symmetric conformer.

$$y = 172.8x - 1.2 \quad \textbf{(Equation 2.6)}$$

$$\ln(K_{eq}) = -\Delta H°/R(1/T) + \Delta S°/R \quad \textbf{(Equation 2.7)}$$

$\Delta H°$: 172.8 = $-\Delta H°/R$; therefore, $\Delta H°$ = -1.4 kJ/mol

$\Delta S°$: -1.2 = $\Delta S°/R$; therefore, $\Delta S°$ = -9.8 J/ mol·K

A proposed mechanism for the olefin-insertion of **1** is shown in Scheme 2.3. The initial step is the attack of the olefin on the metal-hydride, followed by hydride-migration (i). In step two, the remaining bridging hydride is transformed into a terminal hydride, and the nitrogen moiety is rearranged from side-on end-on, to end-on (ii). In the third step, a concerted reaction occurs at the terminal hydride: a second alkene donates electrons from its π orbital into the σ^*_{TaH} orbital; back donation from the σ_{Ta-H} orbital into the π* orbital of the alkene creates a four- centered four-electron transition state (iii). The final step is the insertion of the hydride into the beta position of the alkene, to form an alkyl-transition metal complex (v).

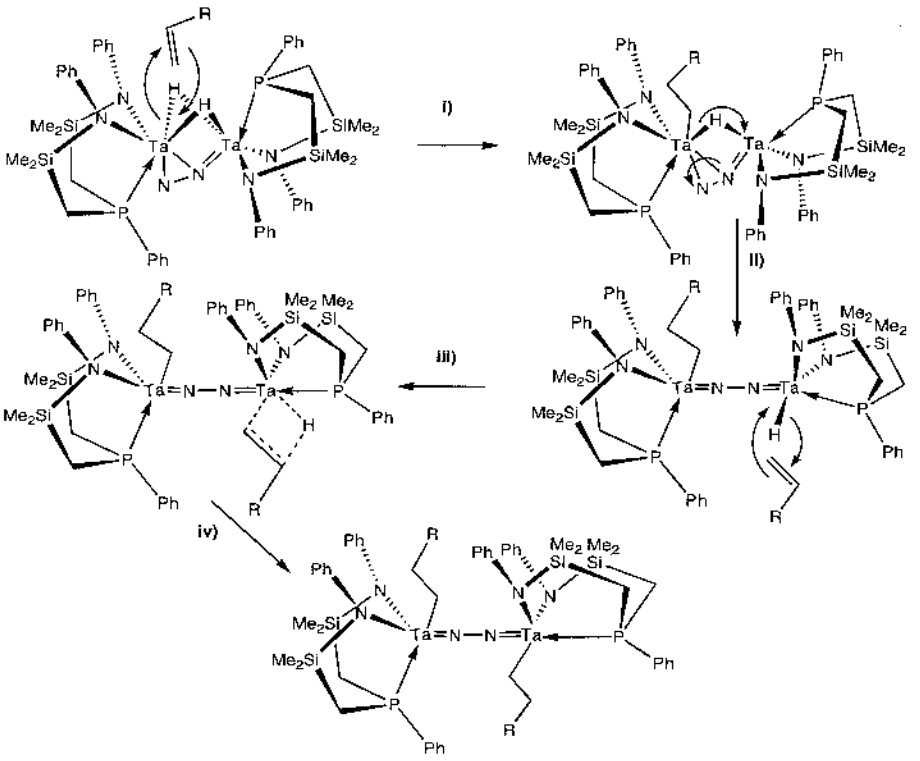

Scheme 2.3

2.4 Conclusions.

The olefin-insertion of **1** with the primary alkenes pentene and hexene produces the pentyl and hexyl complexes **10** and **11**, respectively. The insertion of pentene and hexene with **1** occurs almost immediately and is completed overnight; this is evident from the change in colour of the solution, which turns from dark brown to red.

The NMR spectra of **10** and **11** suggest that they are structurally analogous in solution, with C_s symmetry. The $^{31}P\{^1H\}$ NMR spectra of the $^{15}N_2$ labeled species shows two distinct phosphorus resonances, where only one resonance is coupled to the end-on bound N_2 moiety. The solid-state structure of **11** was analyzed using X-ray diffraction and revealed an end-on bound N_2 unit with an N-N bond length of 1.272(6) Å. In contrast to its symmetry in solution, the solid-state structure of **11** is C_i symmetric. A VT NMR study in conjunction with a Van't Hoff plot revealed that **11** forms an equilibrium between isomers **11A** and **11B** in solution, and that the solid-state structure of **11** was isomer **11B**; however, it is still undetermined as to why this particular isomer is favoured in the solid-state.

2.5 Experimental.

2.5.1. General Procedure.

Unless otherwise stated, all manipulations were performed under an atmosphere of dry, oxygen-free argon or nitrogen by standard Schlenk or glovebox techniques (Vacuum Atmospheres HE-553-2 glovebox equipped with a MO-40-2H purification system and a -35 °C freezer). Ar and N_2 were dried through passage of a column with activated molecular

sieves and MnO. Hexanes, toluene, tetrahydrofuran, pentane, benzene and diethyl ether were purchased anhydrous from Aldrich, sparged with N_2 and passed through columns containing activated alumina and Ridox catalyst. THF-d_8, C_6D_6, and toluene-d_8 were dried over Na/K alloy under partial pressure, trap-to-trap distilled, and freeze-pump-thaw degassed three times. ^1H, $^{31}P\{^1H\}$, ^{13}C, $^1H/^{13}C$-HSQC and $^1H/^1H$-COSY spectra were performed on a Bruker AV-300, Bruker AV-400 or Bruker AV-600 spectrometer, operating at 300.1, 400.0 and 600 MHz respectively. The $^{15}N\{^1H\}$ spectra were performed on a Bruker 600 MHz spectrometer by Dr. Andrew Lewis and Colin Yilin Zhang at the Department of Chemistry at Simon Fraser University. Unless otherwise noted, all spectra were recorded at room temperature. The ^1H, ^{13}C NMR spectra were referenced with C_6D_6 at δ 7.16 and 128.0, respectively. The $^{31}P\{^1H\}$ NMR spectra were referenced to external $P(OMe)_3$ (δ 141.0 with respect to 85% H_3PO_4 at δ 0.0), and the $^{15}N\{^1H\}$ spectra was referenced to an external solution of 100mM NH_4Cl in 90:10 H_2O:D_2O at δ -352.9. Chemical shifts (δ) listed are in ppm, and absolute values of the coupling constants are in Hz. Elemental Analyses were performed by David Wong at the Department of Chemistry at the University of British Columbia.

2.5.2. Materials and Reagents.

Reagents 1-pentene and 1-hexene were purchased from Aldrich and distilled before use. Complexes **1** and $^{15}N_2$-**1** were prepared using literature methods.[69]

2.5.3. Synthesis, Characterization, and Reactivity of Complexes.

Synthesis of ([NPN]Ta(CH$_2$)$_4$CH$_3$)$_2$(μ-η^1:η^1-N$_2$), 10.

A solution of **1** (0.80 g, 0.634 mmol) and 1-pentene (2 mL, 18.28 mmol) in 50 mL benzene was sealed in a glass vessel equipped with a Teflon valve and stirred overnight at 65°C, at which time the colour of the solution changed from dark brown to yellow-red. The vessel was brought into a glovebox where the solvent was removed by vacuum to leave a red residue. The residue was triturated three times with hexanes and decanted. The red solid was collected on a frit 82% yield (0.73 g).

^{1}H NMR (C$_6$D$_6$, 400 MHz): δ 0.08, 0.31, 0.42, and -0.21 (s, 24H total, SiC*H*$_3$), 0.0 (br m, 2H, Ta$_B$C*H*$_2$CH$_2$CH$_2$CH$_2$CH$_3$), 0.92 (t, 3H, Ta$_B$CH$_2$CH$_2$CH$_2$CH$_2$C*H*$_3$), 1.08 (t, 3H, Ta$_A$CH$_2$CH$_2$CH$_2$CH$_2$C*H*$_3$), 1.16 and 1.24 (m, 4H, SiC*H*$_2$P), 1.24 and 1.36 (m, 4H, SiC*H*$_2$P), 1.42 (m, 2H, Ta$_B$CH$_2$ CH$_2$C*H*$_2$CH$_2$CH$_3$), 1.45 (m, 2H, Ta$_B$CH$_2$CH$_2$CH$_2$C*H*$_2$-CH$_3$), 1.51 (m, 2H, Ta$_A$CH$_2$CH$_2$CH$_2$C*H*$_2$CH$_3$), 1.58 (m, 2H, Ta$_A$CH$_2$CH$_2$C*H*$_2$CH$_2$CH$_3$), 1.75 (m, 2H, Ta$_B$CH$_2$C*H*$_2$CH$_2$CH$_2$CH$_3$), 1.83 (m, 2H, Ta$_A$C*H*$_2$CH$_2$CH$_2$CH$_2$CH$_3$), 2.38 (m, 2H, Ta$_A$CH$_2$C*H*$_2$CH$_2$CH$_2$CH$_3$), 6.67, 6.98 (t, 4H, *p*-NC$_6$*H*$_5$), 6.74, 7.32 (m, 8H, *m*-NC$_6$*H*$_5$), 6.91, 7.08 (d, 8H, *o*-NC$_6$*H*$_5$), 7.13, 7.23 (m, 2H, *p*-PC$_6$*H*$_5$), 7.31, 7.48 (m, 4H, *m*-PC$_6$*H*$_5$), 7.74, 7.91 (dd, 4H, *o*-PC$_6$*H*$_5$).

^{31}P{^{1}H} NMR (C$_6$D$_6$): δ 4.69 (s), 20.0 (s).

^{13}C{^{1}H} NMR (C$_6$D$_6$): δ 0.54, 2.16, 4.33, and 6.13 (Si*C*H$_3$), 14.96, and 17.67 (Si*C*H$_2$P), 15.06 (Ta$_B$CH$_2$CH$_2$CH$_2$CH$_2$*C*H$_3$), 15.13 (Ta$_A$CH$_2$CH$_2$CH$_2$CH$_2$*C*H$_3$), 23.33 (Ta$_B$CH$_2$CH$_2$CH$_2$*C*H$_2$CH$_3$), 23.69 (Ta$_A$CH$_2$CH$_2$CH$_2$*C*H$_2$CH$_3$), 27.87 (Ta$_B$CH$_2$*C*H$_2$-CH$_2$CH$_2$CH$_3$), 32.22 (Ta$_A$CH$_2$*C*H$_2$CH$_2$CH$_2$CH$_3$), 39.95 (Ta$_B$CH$_2$CH$_2$*C*H$_2$CH$_2$CH$_3$), 40.91 (Ta$_A$CH$_2$CH$_2$*C*H$_2$CH$_2$CH$_3$), 56.20 (Ta$_A$*C*H$_2$CH$_2$CH$_2$CH$_2$CH$_3$), 73.50 (Ta$_B$CH$_2$-

$CH_2CH_2CH_2CH_3$), 122.15, 122.17 (*p*-NC_6H_5), 128.23, 128.39 (*m*-NC_6H_5), 126.63, 127.77 (*o*-NC_6H_5), 131.01, 130.48 (*p*-PC_6H_5), 129.40, 129.30 (*m*-PC_6H_5), 132.10, 134.53 (*o*-PC_6H_5).

HSQC NMR (C_6D_6): δ (^1H; ^{13}C) (-0.21; 0.54), (0.0; 73.5), (0.8; 2.16), (0.31; 4.33), (0.42; 6.13), (0.92; 15.06), (1.08; 15.13), (1.16; 17.67), (1.24; 17.67), (1.24; 14.96), (1.36; 14.96), (1.42; 27.87), (1.45; 23.33), (1.51; 23.69), (1.58; 32.22), (1.75; 39.95), (1.83; 56.20), (2.38; 40.91), (6.67; 122.15), (6.74; 128.23), (6.91; 126.63), (6.98; 122.17), (7.08; 127.77), (7.13; 131.01), (7.23; 130.48), (7.31; 129.40), (7.32; 128.39), (7.48; 129.30), (7.74; 132.10), (7.91; 134.53).

Analytical Calc'd for $C_{58}H_{84}N_6Si_4Ta_2$: C 49.20; N 6.00; H 6.04; **Found:** *C 45.46; C 6.13; H 6.10.

*All carbon analysis were found to be low, possibly due to the formation of tantalum carbide (TaC).

Synthesis of ([NPN]Ta$(CH_2)_4CH_3)_2(\mu\text{-}\eta^1\text{:}\eta^1\text{-}^{15}N_2)$, 10-$^{15}N_2$.

By the method outlined above, **1-$^{15}N_2$** (0.83 g, 0.658 mmol) and 1-pentene (2 mL, 18.28 mmol) were reacted to obtain 0.70 g of the red product (76% yield).

$^{31}P\{^1H\}$ NMR (C_6D_6): δ 6.81 (dd, $^2J_{PN}$ = 30.4 Hz, $^3J_{PN}$ = 6.5 Hz), 22.1 (s).

^{15}N NMR (C_6D_6): δ 14.13 (dd, $^1J_{NN}$ = 11.5 Hz, $^3J_{PN}$ = 6.5 Hz), 25.92 (dd, $^2J_{PN}$ = 30.4 Hz, $^1J_{NN}$ = 11.5 Hz).

Synthesis of ([NPN]Ta$(CH_2)_5CH_3)_2(\mu\text{-}\eta^1\text{:}\eta^1\text{-}N_2)$, 11.

A mixture of **11** (0.9 g, 0.714 mmol) and 1-hexene (1.5 mL, 12.14 mmol) was stirred in 45 mL of benzene. The dark brown solution was stirred overnight at 65°C and

turned red. The vessel was brought into the glovebox, where the solvent was removed via vacuum and left a red residue that was triturated three times with hexanes, filtered and collected on a glass frit in 86% yield (0.88 g).

^{1}H NMR (C_6D_6, 400 MHz): δ -0.11, 0.10, 0.26, and 0.39 (s, 24H total, SiCH_3), 0.97 and 1.12 (m, 4H, SiCH_2P), 1.12 and 1.37 (m, 4H, SiCH_2P), -0.02 (br m, 2H, $Ta_BCH_2CH_2CH_2CH_2CH_2CH_3$), 0.81 (m, 2H, $Ta_ACH_2CH_2CH_2CH_2CH_2CH_3$), 0.87 (t, 3H, $Ta_ACH_2CH_2CH_2CH_2CH_2CH_3$), 1.14 (m, 2H, $Ta_BCH_2CH_2CH_2CH_2CH_2CH_3$), 1.28 (t, 3H, $Ta_BCH_2CH_2CH_2CH_2CH_2CH_3$), 1.35 (m, 2H, $Ta_ACH_2CH_2CH_2CH_2CH_2CH_3$), 1.61 (m, 2H, $Ta_BCH_2CH_2CH_2CH_2CH_2CH_3$), 1.75 (m, 2H, $Ta_ACH_2CH_2CH_2CH_2CH_2$-CH_3), 1.86 (m, 2H, $Ta_BCH_2CH_2CH_2CH_2CH_2CH_3$), 1.93 (m, 2H, $Ta_BCH_2CH_2CH_2CH_2$-CH_2CH_3), 1.96 (m, 2H, $Ta_ACH_2CH_2CH_2CH_2CH_2CH_3$), 2.39 (m, 2H, $Ta_ACH_2CH_2CH_2$-$CH_2CH_2CH_3$), 6.68, 6.96 (t, 4H, *p*-NC_6H_5), 6.75, 7.34 (m, 8H, *m*-NC_6H_5), 6.93, 7.09 (d, 8H, *o*-NC_6H_5), 7.12, 7.28 (m, 2H, *p*-PC_6H_5), 7.36, 7.51 (m, 4H, *m*-PC_6H_5), 7.78, 7.93 (dd, 4H, *o*-PC_6H_5).

^{31}P{^{1}H} NMR (C_6D_6): δ 6.46, 21.75

^{13}C{^{1}H} NMR (C_6D_6): δ 0.46, 1.73, 4.34, 6.17 (SiCH_3), 14.31, 17.75 (SiCH_2P), 14.68 ($Ta_BCH_2CH_2CH_2CH_2CH_2CH_3$), 15.06 ($Ta_ACH_2CH_2CH_2CH_2CH_2CH_3$), 15.93 ($Ta_BCH_2CH_2CH_2CH_2CH_2CH_3$), 24.00 ($Ta_ACH_2CH_2CH_2CH_2CH_2$-$CH_3$), 28.21 ($Ta_BCH_2CH_2CH_2CH_2CH_2CH_3$), 30.55 ($Ta_ACH_2CH_2CH_2CH_2CH_2CH_3$), 32.07 ($Ta_BCH_2CH_2CH_2CH_2CH_2CH_3$), 32.30 ($Ta_ACH_2CH_2CH_2CH_2CH_2CH_3$), 38.47 ($Ta_BCH_2CH_2CH_2CH_2CH_2CH_3$), 32.63 ($Ta_ACH_2CH_2CH_2CH_2CH_2CH_3$), 63.16 ($Ta_ACH_2CH_2CH_2CH_2CH_2CH_3$), 74.31 ($Ta_BCH_2CH_2CH_2CH_2CH_2CH_3$), 117.12, 118.56

(*p*-NC_6H_5), 122.19, 123.01 (*m*-NC_6H_5), 126.67, 127.02 (*o*-NC_6H_5), 129.94, 130.76 (*p*-PC_6H_5), 129.23, 129.37 (*m*-PC_6H_5), 133.01, 134.23 (*o*-PC_6H_5).

HSQC NMR (C_6D_6): δ (^1H; ^{13}C) (-0.11; 0.46), (1.73; 0.10), (4.34; 0.26), (6.17; 0.39), (0.97; 14.31), (1.12; 14.31), (1.12; 17.75), (1.37; 17.75), (1.28; 14.68), (0.87; 15.06), (1.14; 15.93), (1.35; 24.00), (1.86; 28.21), (0.81; 30.55), (1.93; 32.07), (1.96; 32.30), (1.61; 38.47), (2.39; 32.63), (1.75; 63.16), (-0.02; 74.31), (6.68; 117.12), (6.96; 118.56), (6.75; 122.19), (7.34; 123.01), (6.93; 126.67), (7.09; 127.02), (7.12; 129.94), (7.28; 130.76), (7.36; 129.23), (7.51; 129.37), (7.78; 133.01), (7.93; 134.23).

Synthesis of ([NPN]Ta$(CH_2)_5CH_3)_2(\mu\text{-}\eta^1\text{:}\eta^1\text{-}^{15}N_2)$, 11-$^{15}N_2$.

By the method outlined above, **1-$^{15}N_2$** (0.77 g, 0.610 mmol) and 1-hexene (1.5 mL, 12.14 mmol) were reacted to give 0.63 g (72% yield) of **11-$^{15}N_2$.**

$^{31}P\{^1H\}$ NMR (C_6D_6): δ 6.93 ppm.(dd, $^2J_{PN}$ = 6.5 Hz, $^3J_{PN}$ = 29.5Hz), 22.0 ppm.

^{15}N NMR (C_6D_6): δ 14.15 (dd, $^1J_{NN}$ = 11.3 Hz, $^3J_{PN}$ = 6.5 Hz), 25.94 (dd, $^2J_{PN}$ = 30.4 Hz, $^1J_{NN}$ = 11.3 Hz).

Chapter Three

The Reactivity of Group IV and V Metallocenes with Side-on End-on Coordinated N_2.

3.1 Introduction.

Metallocene dinitrogen complexes, and their reactivity patterns with other reagents have contributed to the current knowledge of N_2 activation and functionalization.[70] Seminal discoveries involved the protonation of early metallocene N_2 complexes to form ammonia and hydrazine.[71,72] For instance, in 1972, Shilov *et al.* reported the formation of ammonia from protonation of $(Cp_2Ti)_2(\mu_2\text{-}\eta^1\text{:}\eta^1\text{-}N_2)$ with HCl.[71] Similarly, Bercaw *et al.* discovered the formation of hydrazine from the reaction of $[(\eta^5\text{-}C_5Me_5)_2ZrN_2]_2(\mu_2\text{-}\eta^1\text{:}\eta^1\text{-}N_2)$ with excess HCl.[3] Inspired by these discoveries, investigations for using metallocene complexes to transform N_2 into useful, organonitrogen products has emerged.

The extent of activation and the bonding mode of N_2 to group IV metallocenes is dictated by the nature of the substituents on the cyclopentadienyl (Cp) ligands (see Figure 3.1).[70] For instance, the reduction of $(\eta^5\text{-}C_5Me_5)_2ZrCl_2$ with sodium amalgam (Na/Hg) in the presence of N_2 forms the end-on bridged dinitrogen complex with two terminal end-on bound dinitrogen units, $[(\eta^5\text{-}C_5Me_5)_2ZrN_2]_2(\mu^2\text{-}\eta^1\text{:}\eta^1\text{-}N_2)$, **A**;[73] in contrast, when the Cp ring has only four methyl substituents, as in $(\eta^5\text{-}C_5Me_4H)_2ZrCl_2$, and is reduced under similar conditions, the side-on N_2 bridged complex, $[(\eta^5C_5Me_4H)_2Zr]_2(\mu_2\text{-}\eta^2\text{:}\eta^2\text{-}N_2)$, **B**, forms.[74] The trend that is apparent in this example is that fewer methyl groups attached to the cyclopentadienyl ring seem to encourage an $\eta^2\text{:}\eta^2\text{-}N_2$ hapticity. This trend is also

observed with the titanocene derivative. N_2 is bound in the end-on bridging mode for both the penta- and tetramethylated Cp complexes $[(\eta^5\text{-}C_5Me_5)_2Ti]_2(\mu^2\text{-}\eta^1\text{:}\eta^1\text{-}N_2)$ (**C**) and $[(\eta^5\text{-}C_5Me_4H)_2Ti]_2(\mu_2\text{-}\eta^1\text{:}\eta^1\text{-}N_2)$, (**D**);[75,76] the side-on bridging N_2 is observed for the trimethylated Cp complex, $[(\eta^5\text{-}C_5H_2\text{-}1,2,4\text{-}Me_3)_2Ti]_2(\mu_2\text{-}\eta^2\text{:}\eta^2\text{-}N_2)$ (**E**).[77]

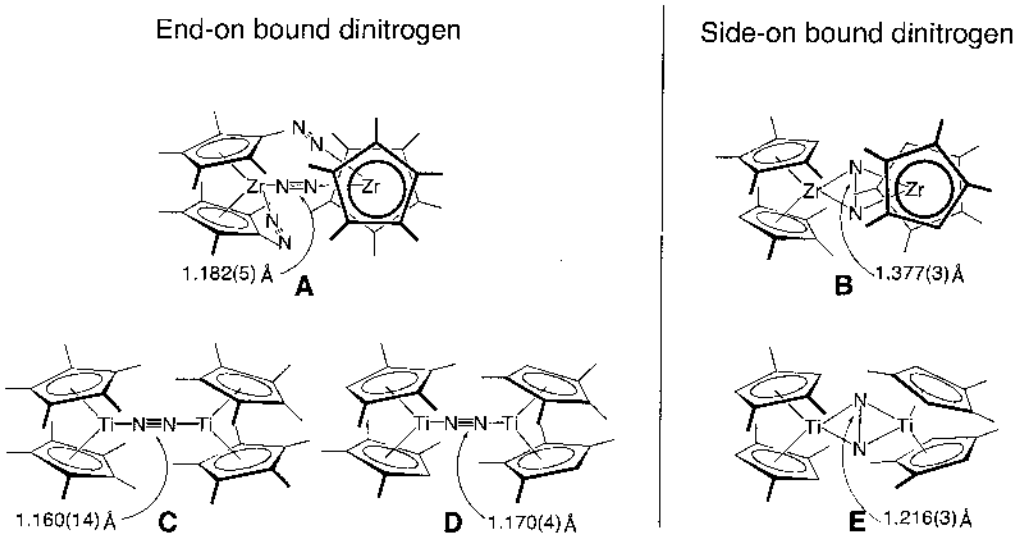

Figure 3.1. Side-on and end-on N_2 zirconocene and titanocene complexes.

Although there are several group IV metallocene dinitrogen complexes, to date, only one example of a group V metallocene-dinitrogen complex is known; the synthesis of complex **F** is shown in Equation 3.1.[78] The reaction of $Cp^*_2TaCl_2$ in THF with sodium amalgam under 1 atm N_2 forms $[(\eta^5\text{-}C_5Me_5)_2TaCl]_2(\mu_2\text{-}\eta^1\text{:}\eta^1\text{-}N_2)$, **F**, which has a moderately activated N_2 unit (N=N = 1.235(13) Å).[78]

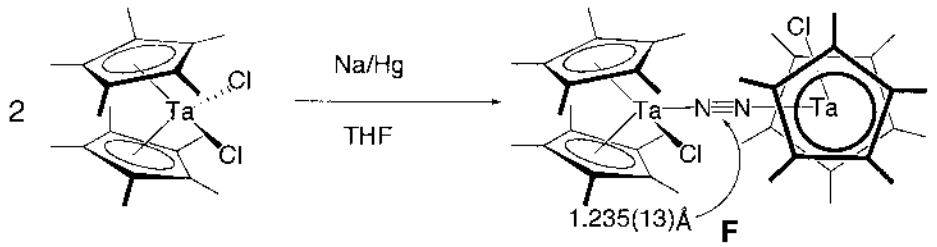

Equation 3.1

Harsh alkali metal reducing agents, such as Na/Hg amalgam or KC_8 under an N_2 atmosphere, are typically employed to generate dinitrogen complexes from a metallocene halide, Cp_2MX_2 (X = Cl or I).[79] In a few cases, dinitrogen complexes have been synthesized without the use of strong reductants via reductive elimination of H_2 from a dihydride complex;[75,77,80] for example, $[(\eta^5\text{-}C_5Me_4H)_2Ti]_2(\mu_2\text{-}\eta^1\text{:}\eta^1\text{-}N_2)$ is formed from $(\eta^5\text{-}C_5Me_4H)_2TiH$ by elimination of H_2 under an N_2 atmosphere.[75] A selection of group IV and V metallocene N_2 complexes, their precursors, and N-N bond lengths (Å) are listed in Table 3.1.

Table 3.1. Group IV and V metallocene dinitrogen complexes, their precursors and N-N bond lengths (Å) (measured via X-ray diffraction).

Precursors	Group IV and V metallocene N2 complexes	N-N bond length (Å)
$[(\eta^5\text{-}C_5H_2\text{-}1,2,4\text{-}Me_3)_2TiH]_n$ or $[(\eta^5\text{-}C_5H_2\text{-}1,2,4\text{-}Me_3)_2TiI]$	$[(\eta^5\text{-}C_5H_2\text{-}1,2,4\text{-}Me_3)_2Ti]_2(\mu_2\text{-}\eta^2\text{:}\eta^2\text{-}N_2)$	1.216(3)[77]
$[(\eta^5\text{-}C_5H_2\text{-}1,2\text{-}Me_2\text{-}4\text{-}^iPr)_2TiI]$	$[(\eta^5\text{-}C_5H_2\text{-}1,2\text{-}Me_2\text{-}4\text{-}^iPr)_2Ti]_2(\mu_2\text{-}\eta^1\text{:}\eta^1\text{-}N_2)$	1.168(3)[77]
rac-$Me_2Si(\eta^5\text{-}C_5H_2\text{-}2\text{-}SiMe_3\text{-}4\text{-}^tBu)_2TiCl_2$	*rac*-$[Me_2Si\text{-}\eta^5\text{-}C_5H_2\text{-}2\text{-}SiMe_3\text{-}4\text{-}^tBu)_2Ti]_2(\mu_2\text{-}\eta^1\text{:}\eta^1\text{-}N_2)$	1.174(3)[77]
$Me_2Si(\eta^5\text{-}C_5Me_4)(\eta^5\text{-}C_5H_3\text{-}3\text{-}^tBu)TiCl_2$	$[Me_2Si(\eta^5\text{-}C_5Me_4)(\eta^5\text{-}C_5H_3\text{-}3\text{-}^tBu)Ti]_2(\mu_2\text{-}\eta^1\text{:}\eta^1\text{-}N_2)$	1.165(3)[77]
$(\eta^5\text{-}C_5Me_4H)_2TiH$	$[(\eta^5\text{-}C_5HMe_4)_2Ti]_2(\mu_2\text{-}\eta^1\text{:}\eta^1\text{-}N_2)$	1.170(4)[75]
$(\eta^5\text{-}C_5Me_5)_2TiCl_2$	$[(\eta^5\text{-}C_5Me_5)_2Ti]_2(\mu_2\text{-}\eta^1\text{:}\eta^1\text{-}N_2)$	1.160(14)[76]
$(\eta^5\text{-}C_5Me_5)_2ZrCl_2$	$[(\eta^5\text{-}C_5Me_5)_2ZrN_2]_2(\mu_2\text{-}\eta^1\text{:}\eta^1\text{-}N_2)$	1.182(5)[73]
$Me_2Si(\eta^5\text{-}C_5Me_4)(\eta^5\text{-}C_5H_3\text{-}3\text{-}^tBu)ZrCl_2$	$[Me_2Si(\eta^5\text{-}C_5Me_4)(\eta^5\text{-}C_5H_3\text{-}3\text{-}^tBu)Zr]_2(\mu_2\text{-}\eta^2\text{:}\eta^2\text{-}N_2)$	1.406(4)[81]
$(\eta^5\text{-}C_5Me_4H)_2ZrCl_2$	$[(\eta^5\text{-}C_5Me_4H)_2Zr(\eta^1\text{-}N_2)]_2(\mu_2\text{-}\eta^2\text{:}\eta^2\text{-}N_2)$	1.377(3)[74]
$Me_2Si(\eta^5\text{-}C_5H_3\text{-}2\text{-}SiMe_3\text{-}4\text{-}CMe_3)_2ZrH_2$	$[Me_2Si(\eta^5\text{-}C_5H_3\text{-}2\text{-}SiMe_3\text{-}4\text{-}CMe_3)_2Zr]_2(\mu_2\text{-}\eta^2\text{:}\eta^2\text{-}N_2)$	1.2450(38)[80]
$(\eta^5\text{-}C_5Me_4H)_2HfI_2$	$[(\eta^5\text{-}C_5Me_4H)_2Hf]_2(\mu_2\text{-}\eta^2\text{:}\eta^2\text{-}N_2)$	1.423(11)[82]
$(\eta^5\text{-}C_5Me_5)_2TaCl_2$	$[(\eta^5\text{-}C_5Me_5)_2TaCl]_2(\mu_2\text{-}\eta^1\text{:}\eta^1\text{-}N_2)$	1.235(13)[78]

3.2 The Chemistry of Cp_2NbH_3 and Cp_2TaH_3.

In this chapter, the reactivity of **1** with group V metallocene hydrides, Cp_2TaH_3 and Cp_2NbH_3 is explored. Cp_2NbH_3 and Cp_2TaH_3 have similar chemical properties, but differ in their reactivity; the former is far more reactive than the latter.[83] For example, in their reactions with $HSiMe_2Ph$, Cp_2TaH_3 requires a higher temperature and longer reaction time compared to Cp_2NbH_3.[84] Structurally, these complexes exhibit a distorted trigonal bipyramidal structure; the two Cp rings are bent back, causing a mixing of the *d*, *s*, and *p* orbitals to form three hybrid orbitals in the equatorial plane (Figure 3.2).[85]

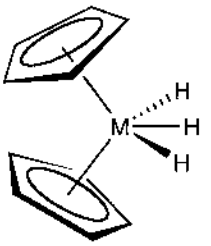

Figure 3.2. An illustration of a group V metallocene hydride.

Heating Cp_2MH_3 (M = Nb or Ta) in the presence of a ligand (L) is a common route to forming Cp_2MHL complexes;[86,87] it is believed that this process occurs via H_2 elimination from Cp_2MH_3 to generate a reactive intermediate, $[Cp_2MH]$, although this intermediate has never been isolated or detected (Equation 3.2).

$$Cp_2MH_3 \rightleftharpoons [Cp_2MH] + H_2$$

Equation 3.2

Some reactions of Cp_2MH_3 are outlined in Scheme 3.1. Heating Cp_2NbH_3 or Cp_2TaH_3 in the presence of triethyl phosphine, carbon monoxide, alkenes and alkynes (L) gives Cp_2MHL.[88] The reaction of $HSiMe_2Ph$ with niobocene and tantalocene hydrides oxidatively adds $HSiMe_2Ph$ to afford the silyl derivatives.[84] When Cp_2NbH_3 or Cp_2TaH_3 are heated in absence of a ligand and eliminate a second equivalent of H_2, a cyclometallated dimer forms.[86]

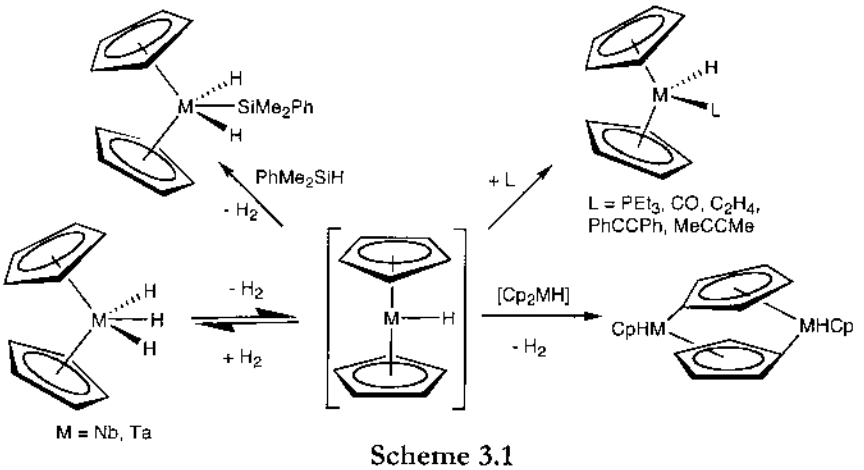

Scheme 3.1

3.3. The Reaction of 1 with $Cp_2Zr(II)$ and $Cp_2Ti(II)$.

As mentioned in Chapter 1, the reaction of **1** with main group hydride reagents (E-H) has previously been studied in the Fryzuk group.[89-92] The extension of this type of E-H addition for metallocene hydrides was of particular interest. The zirconocene hydride reagent, $[Cp_2ZrH_2]_2$, reacts with **1** to give [N(μ-P=N)N]Ta(μ-H)$_2$(μ-N(ZrCp_2))Ta[NPN], **12**, along with the evolution of H_2 (^{1}H NMR (C_6D_6) = δ 4.47) (Equation 3.3).[93] Complex **12** was characterized using X-ray analysis.

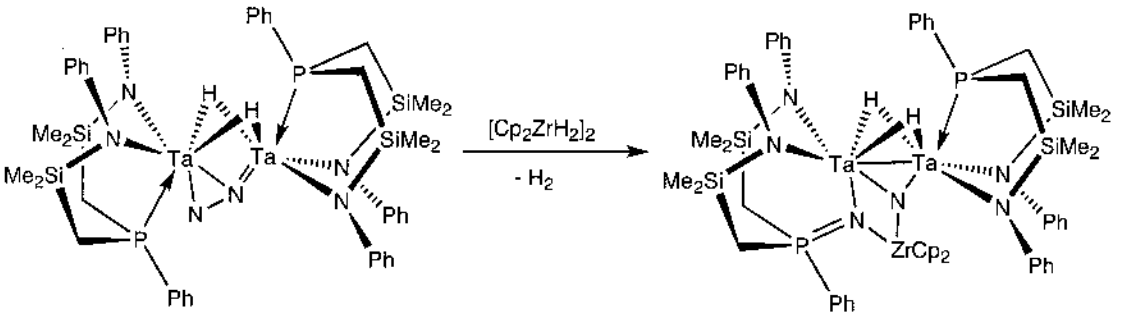

1 **12**

Equation 3.3

To determine the origin of liberated H_2, deuterium labeled **1**, ([NPN]Ta)$_2$(μ-D)$_2$(μ-η^1:η^2-N_2) was reacted with $[Cp_2ZrH_2]_2$; the ^{1}H NMR spectrum revealed free H_2 (no HD), and the formation of **12** with loss of the signal at δ 11.4 due to the two bridging tantalum hydrides. This suggested that there was no HD exchange, and that the source of hydrogen was from $[Cp_2ZrH_2]_2$ to provide a Cp_2Zr(II) species that was responsible for cleaving the N-N bond in **1**. To test this idea, **1** was reacted with a Cp_2Zr(II) precursor, $Cp_2Zr(py)Me_3SiCCSiMe_3$). In this reaction, the formation of **12** was nearly quantitative (90% yield), and strongly suggested that the hydrides of $[Cp_2ZrH_2]_2$ reductively eliminate H_2 to form Cp_2Zr(II) before forming **12**. The reaction of **1** with a Cp_2Ti(II) precursor, $Cp_2Ti(Me_3SiCCSiMe_3)$, was also explored, and produced the analogous complex, **13**, which was characterized by NMR spectroscopy. A proposed mechanism for the formation of **12** and **13** is shown in Scheme 3.2; this mechanism initially involves the formation of an adduct (**B**), followed by an inner-sphere electron transfer to cleave the N-N bond to form a bridging nitride species (**C**), one of which is transformed into a phosphinimide via nucleophilic attack from the phosphine donor in [NPN] (**D**).

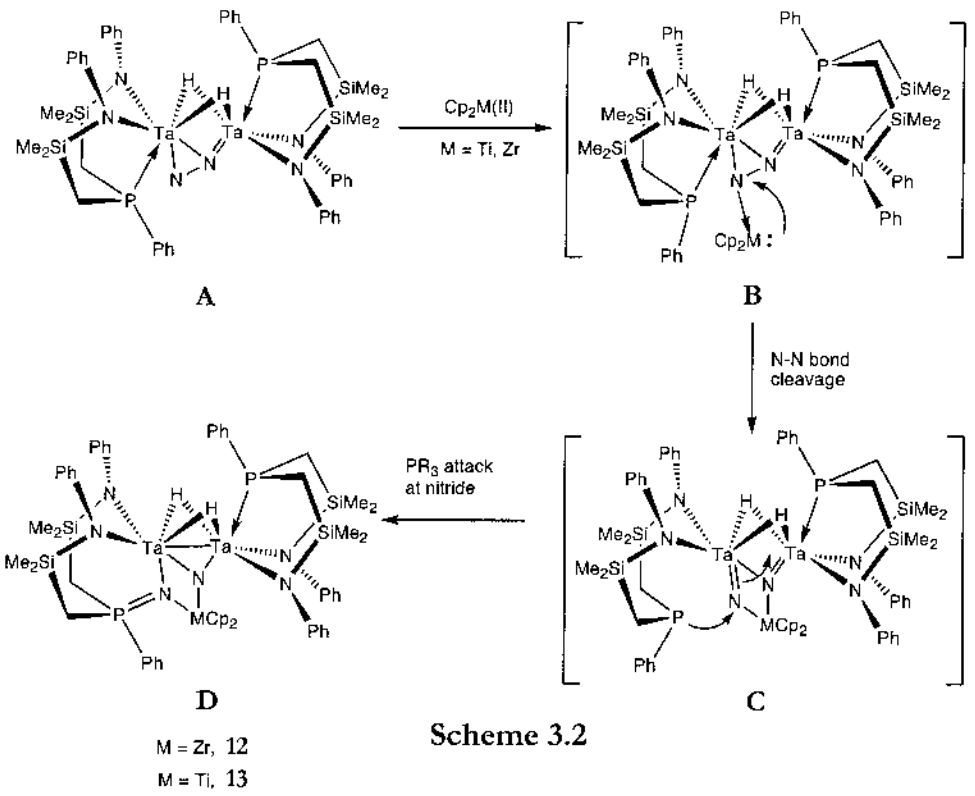

Scheme 3.2

In this chapter, the reaction of **1** with a $Cp_2Hf(II)$ precursor, $Cp_2Hf(PMe_3)(\eta^2$-$Me_3SiCCSiMe_3)$, was explored. In contrast to zirconium and titanium, hafnium has been infrequently used in N_2 activation because it is the most difficult group IV metal to reduce.[94] Only recently has it shown the potential to form highly activated N_2 complexes; for example, extreme lengthening of the N-N bond is observed in hafnium guanidinate and amidinate complexes;[95] also, hafnium N_2 complexes have the tendancy to form the more reactive side-on N_2 complex as opposed to end-on.[94] The reaction of **1** with $Cp_2Hf(PMe_3)(\eta^2$-$Me_3SiCCSiMe_3)$ will be described in section 3.4.1. In addition, the observation that Cp_2ZrH_2 is involved in the cleavage and functionalization of N_2 (described above), led us to investigate the reaction of group V metallocene hydrides, in particular Cp_2TaH_3 and Cp_2NbH_3. Would these metal hydrides undergo the same reductive elimination of H_2 to

generate a $Cp_2MH(III)$ species that would be capable of cleaving and functionalizing N_2 in **1**? These results will be described in section 3.4.2.

3.4. Results and Discussion.

3.4.1. Reaction of 1 with $Cp_2Hf(PMe_3)(\eta^2\text{-}Me_3SiCCSiMe_3)$.

A benzene solution of **1** and $Cp_2Hf(PMe_3)(\eta^2\text{-}Me_3SiCCSiMe_3)$ was heated for three days at 75°C. This generated a dark purple mixture, from which a purple solid, [N(μ-P=N)N]Ta(μ-H)$_2$(μ-N($HfCp_2$))Ta[NPN], **14**, was isolated in 73% yield (Equation 3.4).

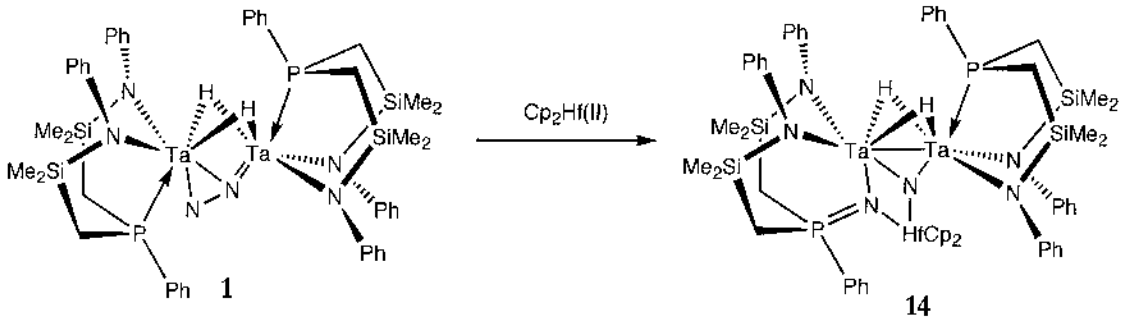

Equation 3.4

The $^{31}P\{^1H\}$ NMR (C_6D_6) spectrum of **14** (Figure 3.3) has two singlet resonances at δ 15.64 and 54.89, indicating that there are two different phosphorus environments. These resonances are similar to those observed for **12** (δ 7.3, 46.7) and **13** (δ 8.6, 46.4).

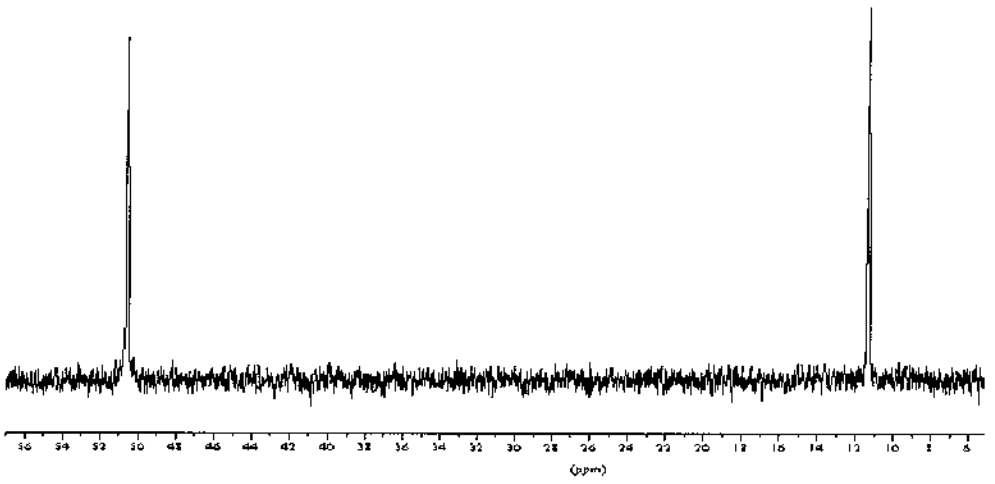

Figure 3.3. $^{31}P\{^{1}H\}$ NMR spectrum of **14** in C_6D_6.

The ^{1}H NMR spectrum of **14** in C_6D_6 shows four inequivalent silyl methyl resonances, a single Cp resonance at δ 5.55, and a doublet for the bridging hydrides at δ 11.48. The $^{15}N_2$ labeled derivative, [N(μ-P=^{15}N)N]Ta(μ-H)$_2$(μ-^{15}N(HfCp$_2$))Ta[NPN], **14**-$^{15}\mathbf{N_2}$, was also prepared. The $^{15}N\{^{1}H\}$ NMR spectrum reveals a doublet at δ -194.3 ($^{1}J_{PN}$ = 31.6 Hz), and a doublet at 204.25 (J_{PN} = 5.6 Hz); these two resonances are not mutually coupled, and implies that N-N cleavage has occurred. The $^{31}P\{^{1}H\}$ NMR spectrum of **14**-$^{15}\mathbf{N_2}$ also shows two resonances: a singlet at δ 11.15, and a doublet at δ 50.43, with a one-bond P-N coupling constant of 31.6 Hz.

Crystals of **14** were grown from an evaporated benzene solution, and analyzed using X-ray diffraction. The solid-state molecular structure of **14**, along with selected bond lengths and bond angles, is shown in Figure 3.4.

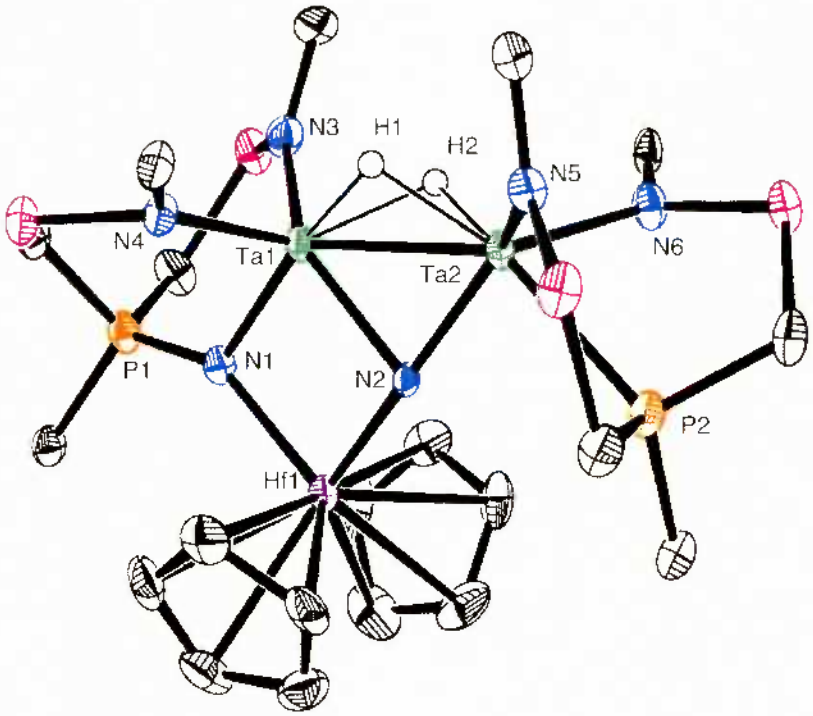

Figure 3.4. An ORTEP depiction of the solid-state molecular structure of **14** (ellipsoids at 50% probability). Hydrides were located on a difference map and refined isotropically. All hydrogen atoms and phenyl ring carbons other than *ipso* carbons have been omitted for clarity. Selected bond lengths (Å) and bond angles (°): Ta1-Ta2 2.6819(4), Ta1-N1 2.094(4), Ta1-N2 2.133(4), Ta2-N2 1.941(4), N1-Hf1 2.110(4), N2-Hf1 2.020(4), N1-P1 1.594(4), Ta1-N3 2.094(4), Ta1-N4 2.057(4), Ta2-N5 2.122(4), Ta2-N6 2.114(4), Ta2-P2 2.6115(14), N1-Ta1-N2 85.95(15), Ta1-N2-Ta2 82.18(14), N1-Hf1-N2 88.47(16), P1-N1-Ta1 121.1(2), P1-N1-Hf1 146.8(3), N3-Ta1-N4 106.96(17), N5-Ta2-N6 105.10(17), Ta1-Ta2-N2 52.00(11).

The solid-state structure of **14** shows a cleaved N_2 unit with a bridging hafnocene fragment between two nitrogen atoms (N1 and N2). Complex **14** is structurally analogous

to **12**; both complexes have a cleaved and functionalized N_2 unit, and a phosphinimide bond (P1=N1). This can suggest that **14** was formed via the same mechanism that was proposed for **12** (Scheme 3.5). The bond lengths of **14** are nearly identical to those of **12**. The Ta1-Ta2 distance is 2.6819(4) Å, similar to other Ta(IV)-Ta(IV) bond lengths that have been reported.[96] The phosphinimide bond length (P1-N1) is 1.594(4) Å, and is within a range that is commonly found for groups 4 and 5 phosphinimide complexes.[97,98] The Hf-N bond lengths (Hf1-N1 = 2.110(4), Hf1-N2 = 2.020(4) Å) are slightly shorter than the Zr-N bond lengths in **12**, (Zr1-N1 = 2.146(9), Zr1-N2 = 2.040(9) Å), as expected.[99]

3.4.2. Attempted Reaction of 1 with Cp_2TaH_3 and Cp_2NbH_3.

A 1:1 mixture of **1** and Cp_2TaH_3 was stirred in d_8-toluene at room temperature for 2 weeks. The reaction was monitored by $^{31}P\{^1H\}$ and ^1H NMR spectroscopy, and no new species were observed by periodically monitoring the reaction over 2 weeks. To promote the loss of H_2 to generate a $[Cp_2TaH]$ species,[100] the same mixture was heated at 100°C for 2 weeks, but produced no visible change. The mixture was also heated under a flow of N_2 for 6 hours, but again there was no change. High-temperature ^1H NMR spectroscopy was also used to monitor the progress of the reaction at 100°C, however, no new products were observed using this technique. The more reactive Cp_2NbH_3[83] was also attempted. A 1:1 mixture of **1** and Cp_2NbH_3 was stirred in benzene at room temperature for 1 week. The progress of the reaction was monitored by $^{31}P\{^1H\}$ and ^1H NMR spectroscopy in C_6D_6, but like the Cp_2TaH_3 reaction above, did not show the formation of any new products. The same mixture was heated and stirred at 90°C for 5 hours under a flow of N_2 to promote the loss of H_2 from Cp_2NbH_3 and form $[Cp_2NbH]$;[101] however, this did not produce any visible

change. High-temperature ^1H NMR spectroscopy at 90°C was also used to observe the progress of the reaction at this temperature, but did not show the formation of any new product.

As mentioned earlier in this chapter, Cp_2MHL complexes are formed by heating Cp_2MH_3 in the presence of a ligand, (L). It is believed that heating Cp_2MH_3 eliminates H_2 to form an equilibrium with a reactive intermediate, $[Cp_2MH]$; however this intermediate has never been isolated or detected. Therefore, a possible explanation for the lack of reactivity between **1** and Cp_2MH_3 might be because the reverse reaction of H_2 with $[Cp_2MH]$ occurs quicker than the reaction between Cp_2MH_3 with **1** (Equation 3.5).

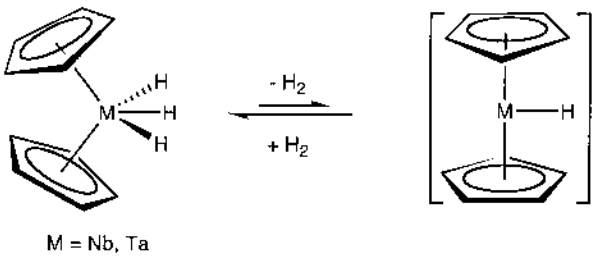

M = Nb, Ta

Equation 3.5

3.5 Conclusions.

The observation that $Cp_2Zr(II)$ reacts with **1** to form **12** compelled us to investigate the reaction of **1** with other group IV and group V metallocene complexes. The reaction of **1** and $Cp_2Hf(PMe_3)(\eta^2\text{-}Me_3SiCCSiMe_3)$ forms **14**, which contains a cleaved and functionalized N_2 unit, and the formation of a new phosphinimide bond. Complexes **12** and **14** are structurally analogous, and it is strongly suggested that both complexes are formed via the same proposed mechansim for **12** (Scheme 3.5).

Unfortunately, the group V metallocene hydrides Cp_2TaH_3 and Cp_2NbH_3 do not react with **1**. Cp_2MH_3 (M = Ta, Nb) was heated to provide a reactive intermediate [Cp_2MH], but no reaction was observed. Since the [Cp_2MH] intermediate cannot be isolated or detected, a possible explanation for lack of reactivity between **1** and Cp_2MH_3, might be because the reverse reaction of H_2 and [Cp_2MH] occurs quicker than the forward reaction of [Cp_2MH] and **1**.

3.6 Experimental.

3.6.1. General Procedure.

Unless otherwise stated, general procedures were performed as described in Section 2.4.1.

3.6.2. Materials and Reagents.

$Cp_2Hf(PMe_3)(\eta^2\text{-}Me_3SiC_2SiMe_3)$,[102] **1**[103] and $^{15}N_2$-**1**[103] were prepared using literature methods.

3.6.3. Synthesis, Characterization, and Reactivity of Complexes.

Synthesis of [N(μ-P=N)N]Ta(μ-H)$_2$(μ-N(HfCp$_2$))Ta[NPN], 12.

([NPN]Ta(μ-H)$_2$(μ-η^1: η^1-N_2) (0.65g, 0.515 mmol) and $Cp_2Hf(\eta^2\text{-}Me_3SiCC\text{-}SiMe_3)$ (0.29g, 0.515 mmol) was dissolved in 50 mL benzene at room temperature, and sealed in a glass vessel equipped with a Teflon valve. The brown mixture was stirred for three days at 75°C, and the colour of the solution changed from brown to purple. The vessel was brought into a glovebox and the solvent was removed under vacuum, leaving a purple residue

that was triturated with hexanes and filtered to collect a purple powder, **14** (Yield = 0.59 g, 73%).

^{1}H NMR (C_6D_6, 25°C, 400 MHz): -0.13, 0.12, 0.19, 0.28 (s, 6H each, SiCH_3), 1.32 (dd, $^2J_{HH}$ = 10.9 Hz, $^2J_{PH}$ = 22.5 Hz, 4H, SiCH_2P), 1.94 (dd, $^2J_{HH}$ = 14.0 Hz, $^2J_{PH}$ = 39.2 Hz, 4H, SiCH_2P), 5.54 (s, 10H, η^5-C_5H_5), 6.52, 6.76, 6.99, 7.08, 7.29 (d, t, 20H total, NC$_6H_6$), 7.13, 7.21, 7.26, 7.38 (d, t, 6H total, PC$_6H_6$), 7.54, 7.88 (dd, 4H, *o*-PC$_6H_6$) 11.48 (d, 2H, $^2J_{Ta-H}$ = 16.6 Hz)

^{31}P{^{1}H} NMR (C_6D_6): δ 15.64 (s) 54.89 (s).

^{13}C{^{1}H} NMR (C_6D_6): 0.33, 3.75, 4.44, 5.18 (SiCH_3), 14.6, 20.33 (SiCH_2P), 108.63, (η^5-C_5H_5), 117.10, 118.53, 120.56, 122.86, 126.67, 129.51 (NC_6H_6), 129.02, 129.27, 129.95, 131.30 (PC$_6H_6$), 131.83, 133.42 (*o*-PC_6H_6).

Analytical Calc'd for $C_{58}H_{74}N_6P_2Si_4Ta_2Hf$: C 44.37; H 4.75; N 5.35; **Found:** C 44.67; H 5.11; *N 4.81.

*Nitrogen analysis were found to be low, possibly due to the formation of HfN or TaN.

Synthesis of [N(μ-P=^{15}N)N]Ta(μ-H)$_2$(μ-^{15}N(HfCp$_2$))Ta[NPN], 12-$^{15}N_2$.

By the same method outlined above, **1-$^{15}N_2$** (0.88 g, 0.698 mmol) and $Cp_2Hf(\eta^2$-$Me_3SiC_2SiMe_3)$ (0.393 g, 0.698 mmol) were reacted to give (0.84 g, 87% yield) of **12-$^{15}N_2$**.

^{31}P{^{1}H} NMR (C_6D_6): δ 11.15 (s), 50.43 (d, $^1J_{PN}$ = 31.6 Hz).

^{15}N NMR (C_6D_6): δ -194.3 (d, $^1J_{PN}$ = 31.6 Hz), 204.25 (d, J_{PN} = 5.6 Hz).

3.6.4. Attempted Reactions of 1 and Cp_2MH_3.

Complex **1** (102 mg, 0.08 mmol) and Cp_2MH_3 (1 equivalent) was dissolved in 1.5 mL in toluene and sealed in a J-Young tube and heated at 100°C (for M = Ta) and 90°C (for M = Nb).

Complex **1** (1 g, 0.8 mmol) and Cp_2 MH_3 (1 equivalent) was dissolved in toluene and heated at 100°C for 6 hours (M = Ta) and 90°C for 5 hours (M = Nb) under a flow of N_2.

Chapter Four

The Reactivity of a Group 13 Complex with Side-on End-on coordinated N_2.

4.1 Introduction.

When nitrogen is activated in a transition-metal complex, the N_2 unit may be susceptible to electrophilic attack. The most common electrophilic addition reaction with coordinated dinitrogen is protonation.[104] Protonation of transition-metal N_2 complexes is of interest because it is invoked in biological nitrogen fixation.[105,106] One example of a homogeneous catalyst that is capable reducing and protonating dinitrogen to ammonia is the mononuclear molybdenum complex, $[HIPTN_3N]Mo(N_2)$, ($[HIPTN_3N]^{3-}$ = [{3,5-(2,4,6-i-Pr_3-C_6H_2)$_2$$C_6H_3NCH_2CH_2$}$_3$N]$^{3-}$) shown below.[107] This complex contains a tetradentate triamidoamine ligand, and can reduce N_2 to NH_3 under ambient conditions (at room temperature and 1 atmospheric pressure).

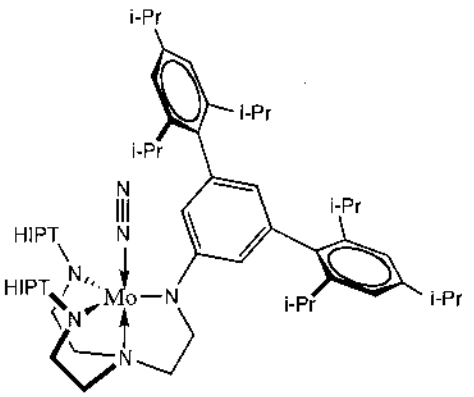

The catalytic production of organonitrogen compounds from molecular nitrogen has become a "holy grail" in dinitrogen research;[108] thus, in addition to protonation reactions, the reactions of coordinated N_2 with other electrophilic reagents have also been explored. Some reactions of N_2 complexes with group 13 electrophiles, (E), afford new N-E bonds. For example, *cis*-$[W(N_2)_2(L)_3L_1]$ (**A**) reacts with $GaCl_3$[109] and $AlCl_3$[110] to form *trans,trans*-$[\{WCl(PMe_2Ph)_4(\mu_3\text{-}N_2)\}_2(GaCl_2)_2]$(N-N = 1.32(2) Å) (**B**) and $[WCl(Py)(PMe_2\text{-}Ph)_3(\mu_3\text{-}N_2)]_2(AlCl_2)_2$ (N-N = 1.46(4) and 1.25(3) Å) (**C**), respectively; the reaction of *trans*-$[NBu_4][W(NCS)(N_2)(dppe)_2]$ (**D**) with $H_2BCMe_2CHMe_2$[111] forms the boryldiazenido complex, *trans*-$[W(NCS)(N{=}NBHCMe_2CHMe_2)(dppe)_2]$ (N-N = 1.262(7) Å) (**E**). These reactions are illustrated in Scheme 4.1.

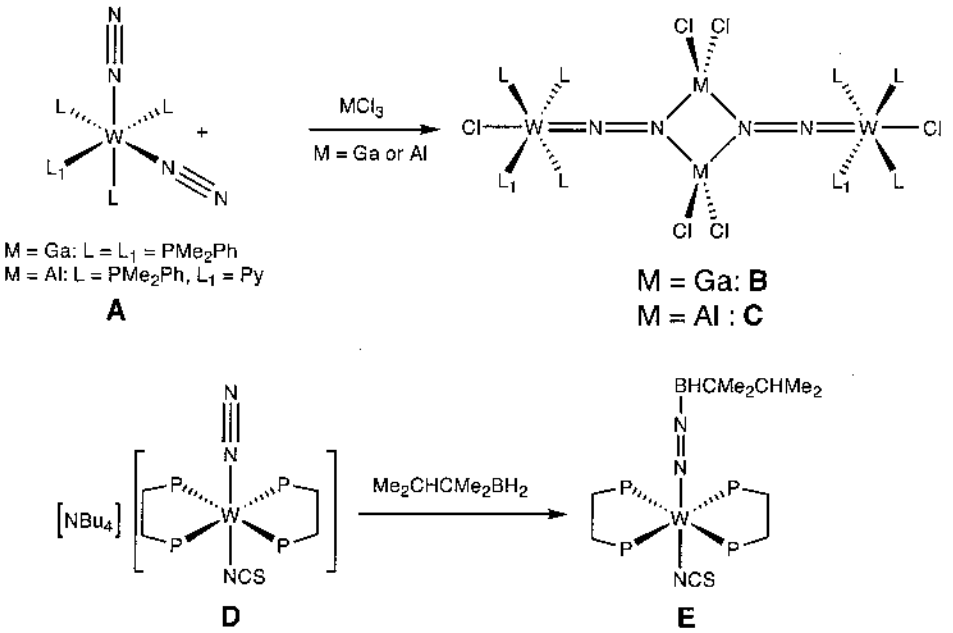

Scheme 4.1

Electrophilic group 14 complexes can also react with coordinated dinitrogen (see Scheme 4.2). For instance, the reaction of *trans*-$[W(N_2)_2(dppe)_2]$ (**A**) with alkyl bromides

and acyl chlorides forms new N-C bond complexes (**B** and **C**).[112,113] Silicon electrophiles can react with coordinated N_2 to form N-Si bonds; the reaction of *cis*-$[W(N_2)_2(dppe)_2]$ (**D**) with Me_3SiI affords a silyldiazenido complex, *trans*-$[WI(NNSiMe_3)(PMe_2Ph)_4]$ (**E**);[114] similarly, the reduction of $[N_3N]MoCl$ ($[N_3N = N(CH_2CH_2NSiMe_3)_3$) (**F**) with magnesium generates $\{[N_3N]Mo\text{-}N{=}N\}_2Mg(THF)_2$, which reacts with Me_3SiCl to form $[N_3N]MoN{=}NSiMe_3$ (**G**).[115]

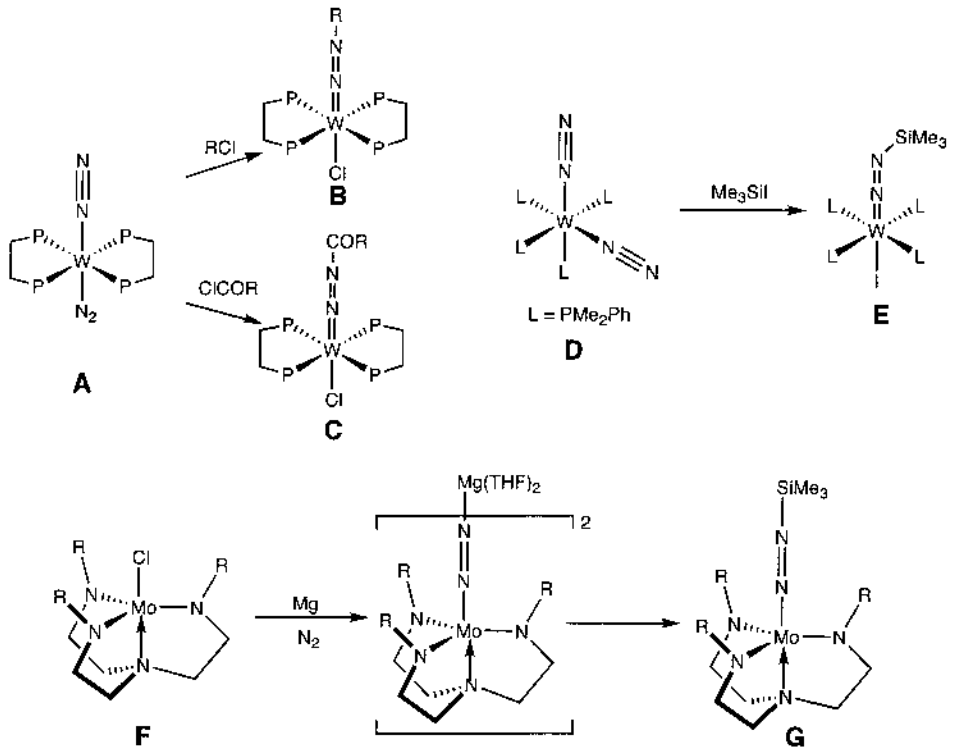

Scheme 4.2

4.2. Reaction of 1 with Lewis Acids.

Lewis acids XR_3, (XR_3 = $AlMe_3$ (**15**), $GaMe_3$ (**16**), and $B(C_6F_5)_3$ (**17**) react with **1** to form the adducts, $[(NPN)Ta]_2(\mu\text{-}H)_2(\mu\text{-}\eta^1{:}\eta^2\text{-}NNXR_3)$ (see Equation 4.1).[116] The solid-state structures of **15**, **16**, and **17** have N-N bond lengths longer than that of **1**, at

1.363(7), 1.356(18), and 1.393(7) Å, respectively. In this chapter, the reactivity of **1** with GaCp* is explored.

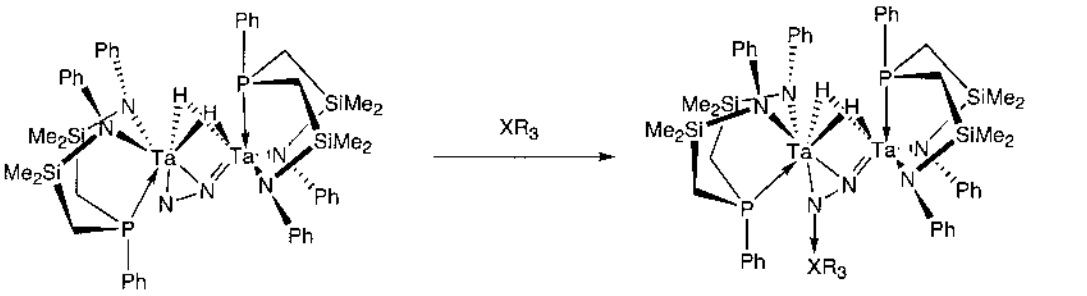

1 $XR_3 = AlMe_3$ (**15**), $GaMe_3$ (**16**), $B(C_6F_5)_3$ (**17**)

Equation 4.1.

4.3. Results and Discussion.

4.3.1. Reaction of 1 with GaCp*.

The initial reaction of **1** and GaCp* (1:1 equivalent) at room temperature is immediate but incomplete, as indicated by $^{31}P\{^1H\}$ NMR spectroscopy (Figure 4.1); in addition to the resonances of **1** (δ 11.7 and 13.8), the $^{31}P\{^1H\}$ NMR spectrum shows two doublets at δ 14.3 and 22.3 (J_{pp} = 14.67 Hz), that are reminiscent of the $^{31}P\{^1H\}$ NMR spectrum of the adduct complex $[(NPN)Ta]_2(\mu\text{-}H)_2(\mu\text{-}\eta^1\text{:}\eta^2\text{-}NNGaMe_3)$, **16**.

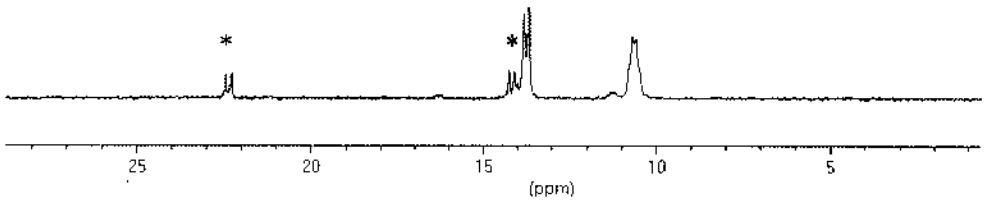

Figure 4.1. $^{31}P\{^{1}H\}$ NMR spectrum of **1** and GaCp* in C_6D_6. The two new doublets are represented by (*).

Since the reaction is not complete after stirring for several days at room temperature, the same mixture was heated overnight at 65°C. This resulted in the conversion of **1** into a new complex, [NPN]Ta(μ-N(GaCp*))Ta(=NPh)[NPμ-N], **18**. Attempts to isolate **18** were unsuccessful; however, the complex was characterized *in situ* using $^{1}H/^{13}C$-HSQC, $^{13}C\{^{1}H\}$, $^{31}P\{^{1}H\}$ and $^{15}N\{^{1}H\}$ NMR spectroscopy, and based on the data provided by these spectra, a proposed structure for **18** is shown in Equation 4.2.

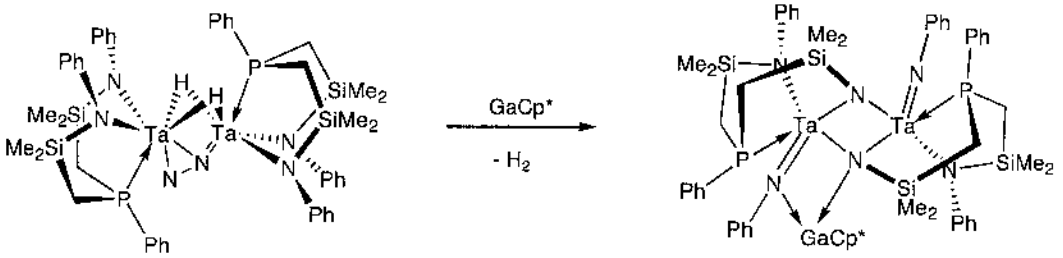

1 **18**

Equation 4.2.

The $^{31}P\{^{1}H\}$ NMR spectrum of **18** no longer shows the two mutually coupled doublets that were observed at the onset of the reaction (i.e. Figure 4.1), but reveal two new singlets at δ -2.65 and 20.38, indicative of two different ^{31}P environments (Figure 4.2). The ^{1}H NMR spectrum of **18** shows no peaks in the region where the resonances for the bridging hydrides typically occur (at ~δ 11), but show eight singlets assigned to silyl methyl protons, and a singlet at δ 1.89 assigned to GaCp* protons (Figure 4.3); these findings suggest that **18** is C_1 symmetric in solution. Since **1** does not decompose or eliminate H_2 even in refluxing in toluene, the loss of the bridging hydrides in the formation of **18** appears to require heating **1** in the presence of GaCp*.

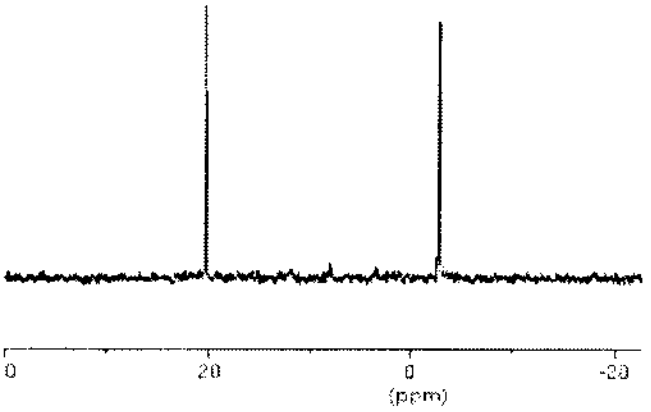

Figure 4.2. $^{31}P\{^{1}H\}$ NMR spectrum of **18** in C_6D_6.

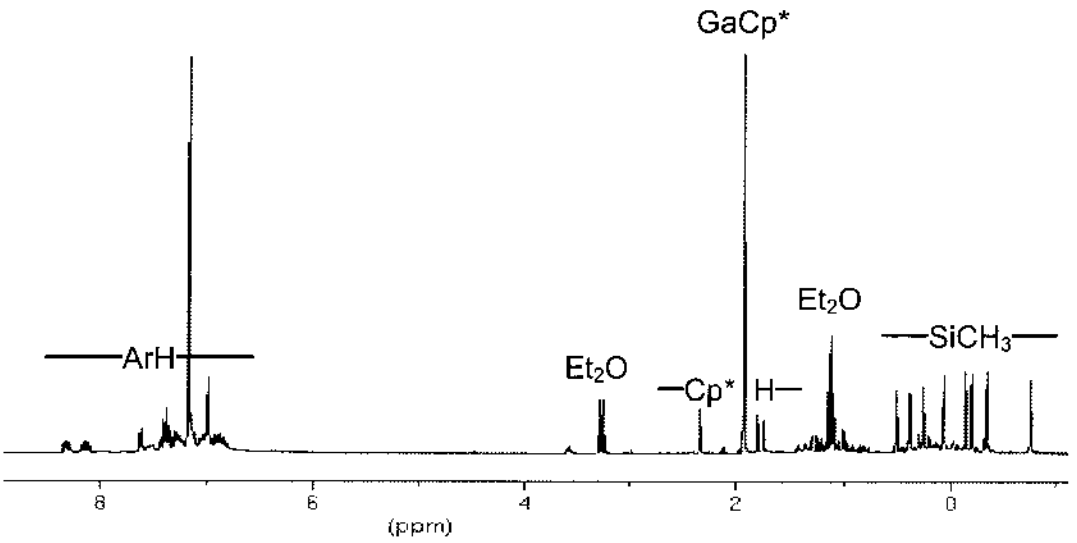

Figure 4.3. 400 MHz ^{1}H NMR (C_6D_6) spectrum of **18**. The trace amount of Et_2O is an impurity in the deuterated solvent.

The $^{15}N_2$ labeled derivative, [NPN]Ta(μ-^{15}N(GaCp*))Ta(=NPh)[NPμ-^{15}N], **18-$^{15}N_2$**, was also prepared and characterized by NMR spectroscopy, and supports the structure proposed for **18** in Equation 4.3. The ^{31}P{^{1}H} NMR spectrum of **18-$^{15}N_2$** shows two doublets at δ -0.97 ($^2J_{PN}$ = 19.27 Hz) and 22.08 ($^2J_{PN}$ = 11.06 Hz); these resonances are different from those reported for the metallocene complexes **12**, **13**, and **14** in Chapter 3, which show only one ^{31}P resonance coupled to an ^{15}N nucleus and indicates that **18** is structurally different from these complexes. The ^{15}N{^{1}H} NMR spectrum (Figure 4.4) shows two doublet of doublets at δ -23.2 ($^2J_{PN}$ = 19.27 Hz, $^1J_{NSi}$ = 3.01Hz) and at δ 291.2 ($^2J_{PN}$ = 11.06 Hz, $^1J_{NSi}$ = 2.01 Hz); these values are in contrast to those reported for **1-$^{15}N_2$**, at δ -20.4 (J_{NP} = 6.6, 24.6 Hz; J_{NN} = 21.6 Hz) and 163.6 (J_{NP} = 3.5, 21.2 Hz; J_{NN} = 21.6)),

indicating that the side-on end-on N_2 in **1** has changed in **18**. Furthermore, the splitting in the $^{15}N\{^1H\}$ NMR resonances of **18** reveals two different nitrogen atoms that are not mutually coupled, but coupled to different phosphorus and silicon environments (the $^2J_{PN}$ and $^1J_{NSi}$ values found herein are within the range of other [NPN] complexes that have a similar structure to **18** and exhibit a two-bond N-P and one-bond N-Si coupling)[16] implying that N-N bond cleavage has occurred, and that each ^{15}N atom has a unique chemical environment, thereby supporting the structure proposed for **18** in Equation 4.3.

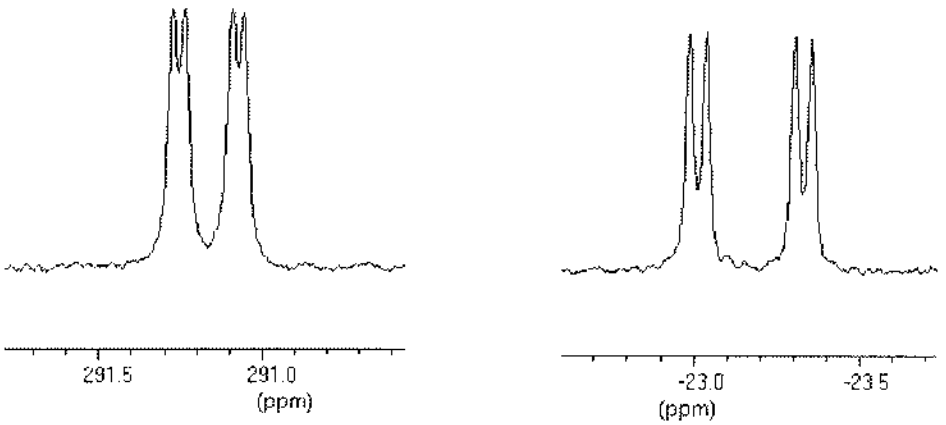

Figure 4.4 $^{15}N\{^1H\}$ NMR resonances of **18** in C_6D_6.

Complex **18** is unstable in solution, and can be observed by $^{31}P\{^1H\}$ NMR spectroscopy to convert into a number of other P-containing species over several days. One of the products of this reaction was determined to be $[(PhN)(NP\mu\text{-}N)Ta]_2$, **19**. The solid-state molecular structure of **19** was established by X-ray crystallography (Figure 4.5), and can support the structure of **18** proposed in Equation 4.3.

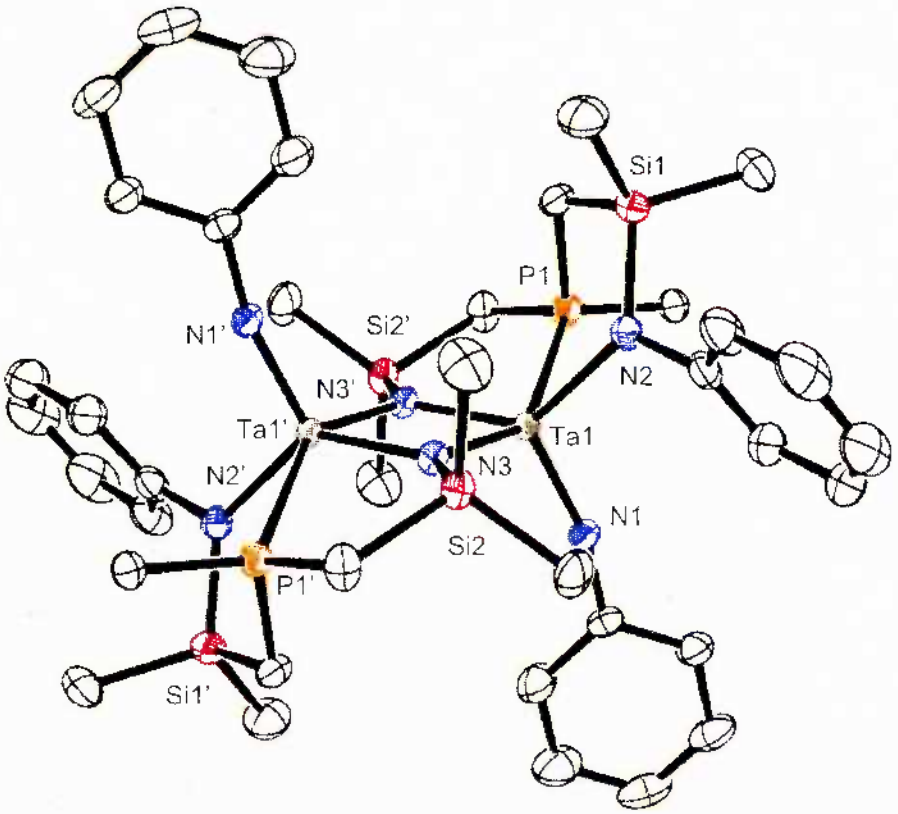

Figure 4.5. An ORTEP depiction of the solid-state molecular structure of **19** (ellipsoids at 50% probability). All silyl methyl groups, hydrogen atoms and phenyl ring carbons other than *ipso* carbons have been omitted for clarity. Selected bond lengths (Å) and bond angles (°): Ta1-Ta1' 3.0878(5), Ta1-N3 2.0264(15), Ta1-N1 1.8006(16), Ta1-N2 2.0686(16), Ta1-P1 2.6172(6), N3-Si2 1.1776(16), N3-Ta1-N3' 80.82(6), N3-Ta1-N2 103.48(6), N1-Ta1-N3 109.99(7), N3-Ta1-P1 146.19(15), N1-Ta1-P1 101.35(5), N1-Ta1-N2 108.97(7), Si2-N3-Ta1 129.06(9), Ta1-N3-Ta1' 99.18(6).

The geometry about the tantalum center is best described as distorted square pyramidal, with the axial position occupied by N1, and the base vertices occupied by P1, N2, N3 and N3'. Decomposition of the [NPN] ligand at the N-Si bond is evident from the

structure. A square M_2N_2 unit (M = Ta) is also apparent in the solid-state, and is a shape that has previously been observed with other group V N_2 complexes.[117,118]

The solid-state structure of **19** has a center of inversion, and it is apparent that there is no GaCp* in the complex. It is possible that GaCp* is responsible for the different symmetry observed between complexes **18** and **19**, and that complex **18** is merely a GaCp* adduct of **19**. The solid-state structure of **19** shows a cleaved N-N bond where the bridging N atoms are each bound to an Si atom; the $^{15}N\{^1H\}$ NMR spectrum of **18** shows two distinct ^{15}N environments that each display $J_{N\text{-}Si}$ coupling, and support the formation of a N-Si bond, like **19**. The ^1H NMR spectrum of **18** also shows loss of the bridging hydride resonance at δ 11.4, and is in agreement with the solid-state structure of **19**, which shows no bridging hydride atoms. Therefore, the bonding information provided by the solid-state structure of **19** further supports the structure of **18** proposed in Equation 4.3.

Decomposition of the [NPN] ligand at the N-Si bond has previously been observed with hydroboration reactions of **1** (Equation 4.3) with $HB(C_6H_{11})_2$ (**20**) and 9-BBN (**21**).[119] The mechanism for this process has been investigated by MacKay *et al.*;[119] the reaction of deuterium labeled **1**, $([NPN]Ta)_2(\mu\text{-}D)_2(\mu\text{-}\eta^1\text{:}\eta^2\text{-}N_2)$, with 9-BBN and $HB(C_6H_6)$ revealed that N-N bond cleavage in **1** was correlated to H_2 elimination from the bridging hydrides; ^{15}N NMR studies revealed that the bridging nitrogen atoms in **20** and **21** originated from the side-on end-on N_2 in **1**; ^{29}Si NMR studies showed that the Si atom from [NPN] migrates to the bridging N atom.

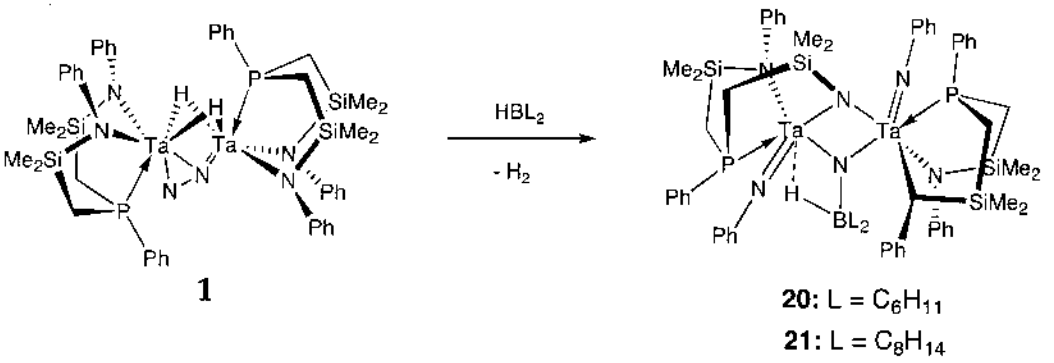

Equation 4.3

4.4. Conclusions.

The reaction of **1** with GaCp* results in a cleaved and functionalized N_2 complex, [NPN]Ta(μ-N(GaCp*))Ta(=NPh)[NPμ-N], **18**. Although **18** could not be isolated, a possible solution structure was assigned by NMR spectroscopy and isotopic labeling. Complex **18** converts to **19**, [(PhN)(NPμ-N)Ta]$_2$, spontaneously in solution over several days. Both **18** and **19** have undergone ligand decomposition, most likely because of the reactivity of the N-Si bond in [NPN]; Si is bound to the bridging nitride, and a phenylamide group is bound to Ta. A similar decomposition of [NPN] has been observed upon hydroboration of **1**, and it is presumed that the formation of complex **18** and **19** occurs through a similar mechanism.

4.5 Summary and Future Work.

This thesis investigates the reactivity of the tantalum dinitrogen complex, ([NPN]Ta)$_2$(μ-H)$_2$(μ-η^1:η^2-N_2), **1**, with primary alkenes, group IV and V metallocenes, and with GaCp*. In Chapter 2, the reaction of **1** with the 1-pentene and 1-hexene produced

([NPN]Ta$(CH_2)_4CH_3)_2(\mu\text{-}\eta^1\text{:}\eta^1\text{-}N_2)$, **10**, and ([NPN]Ta$(CH_2)_5CH_3)_2(\mu\text{-}\eta^1\text{:}\eta^1\text{-}N_2)$, **11**, each with two new Ta-C bonds, and a change to the bonding mode of N_2 in **1**. This reaction likely occurs through the olefin-insertion of the primary alkene into the Ta-H bond. Complexes **10** and **11** were characterized by NMR spectroscopy, and the solid-state structure of **11** revealed that the N_2 unit is in the bridging end-on mode, with an N-N bond length of 1.272(6) Å. The symmetry of **11** in solution is different from its symmetry in the solid-state. Complex **11** forms two isomers in solution; **11A** which is the C_s isomer and the predominant isomer in solution at room temperature, and **11B**, which is the minor C_i isomer. Therefore, the solid-state structure represents isomer **11B**, although it is unclear as to why this particular isomer is favoured in the solid-state.

In Chapter 3 the reactivity of **1** with group IV and V metallocenes was investigated. The reaction of **1** with $Cp_2Hf(PMe_3)(\eta^2\text{-}Me_3SiCCSiMe_3)$ produces [N(μ-P=N)N]Ta(μ-$H)_2$(μ-N(HfCp_2))Ta[NPN], **14**, in which N_2 is cleaved and new Hf-N and P=N bonds have formed. The cleavage of N_2 in **1** may be accomplished by the donation of two electrons from a Cp_2Hf(II) species. In addition, the reaction of **1** with group V metallocene hydrides Cp_2MH_3 (M = Nb, Ta) was attempted, however, no reaction was observed. It is believed that the 16 electron intermediate, [Cp_2MH(III)] reacts quicker with H_2 than with **1**, and does not produce any useful result.

In Chapter Four, the reaction of **1** with GaCp* to produce [NPN]Ta(μ-N(GaCp*))Ta(=NPh)[NPμ-N], **18**, was reported. Complex **18** decomposes over several days, and one product of decomposition that was isolated was [(PhN)(NPμ-N)Ta]$_2$, **19**. The solid-state structure of **19** showed that the [NPN] ligand was cleaved at the N-Si bond, similar to that observed for the reaction of **1** with 9-BBN and $HB(C_6H_5)_2$.

This thesis has discussed the reaction of **1** with some early transition metal complexes in Chapter 4. In addition to many other reactions of **1** with early transition-metal complexes that remain to be explored, the reaction of **1** with certain late-transition metal complexes should be attempted. For example, $Pd_2(dba)_3$ or $(COD)_2Ni$ may form adduct complexes or cleave and functionalize N_2 in **1**. The reaction of **1** with other organic reagents such as cyclic alkenes and allenes and is another area that can be explored, and may possibly result in the formation of a carbon-nitrogen bond.

4.6. Experimental.

4.6.1. General Procedure.

Unless otherwise stated, general procedures were performed as described in Section 2.4.1.

4.6.2. Materials and Reagents.

GaCp*,[120] **1**[121] and $^{15}N_2$-**1**[121] were prepared using literature methods.

4.6.3. Synthesis, Characterization, and Reactivity of Complexes.

Synthesis of [NPN]Ta(μ-N(GaCp*))Ta(=NPh)[NPμ-N], 18.

GaCp* (16.5 mg, 0.081 mmol) was added dropwise to a solution of **1** (102 mg, 0.081 mmol) in 1.5 mL of C_6D_6 at room temperature. The mixture was sealed in a J-Young tube and heated overnight at 65°C.

^{1}H NMR (C_6D_6, 400 MHz): -0.78, -0.34, -0.19. -0.16, 0.08, 0.27, 0.39, 0.51 (s, 3H each, SiCH_3), 0.78, 0.88, 1.05, 1.26 (m, 2H each, SiCH_2P), 1.98 (s, 15H, $GaC_{10}H_{15}$), 6.81,

6.84, 6.87, 6.92, 6.94, 6.96, 7.01, 7.05, 7.08, 7.23, 7.30, 7.38, 7.42 (d, t, 20H, NC_6H_5), 7.53, 7.66, 8.15, 8.38 (m, dd, 10H, PC_6H_5).

$^{31}P\{^1H\}$ NMR (C_6D_6, 161 MHz): δ -2.65 (*s*) 20.38 (s).

$^{13}C\{^1H\}$ NMR (C_6D_6, 101 MHz): 0.05, 1.29, 2.11, 2.46, 3.12, 3.27, 5.28, 6.57 ($SiCH_3$), 10.3 ($GaC_5(C_5H_{15})$), 113.4 ($GaC_5(C_5H_{15})$), 13.6, 15.8, 20.4, 21.8 ($SiCH_2P$), 119.6, 121.8, 121.3, 121.9, 122.1, 123.5, 124.1, 125.7, 125.9, 129.1, 129.4, 129.8, 131.3 (phenyl ring carbons), 131.8, 133.7, 134.3 and 135.2 (PC_6H_5). *Note some proton and carbon resonances were eclipsed by solvent.

$^1H/^{13}C$ HSQC NMR (C_6D_6): δ (^1H; ^{13}C) (-0.78; 2.11), (-0.34; 1.29), (-0.16; 2.46), (0.08; 0.05), (0.27; 3.12), (0.39; 5.38), (0.51; 6.57); (0.78; 13.6), (0.33; 20.4), (1.05; 21.8), (1.26; 15.8); (1.98; 10.3); (6.81; 121.8), (6.84; 122.1), (6.87; 119.6), (6.92; 123.5), (6.94; 119.6), (6.96; 124.1), (7.01; 121.9), (7.05; 125.9), (7.08; 129.1), (7.23; 129.4), (7.30; 131.3), (7.38; 129.8), (7.53; 131.8), (7.66; 133.7), (8.15; 134.3), (8.38; 135.2).

Synthesis of [NPN]Ta(μ-^{15}N(GaCp*))Ta(=NPh)[NPμ-^{15}N], 18-$^{15}N_2$.

By the method outlined above, **1-$^{15}N_2$** (0.93 g, 0.737 mmol) and GaCp* (0.151 g, 0.737 mmol) were reacted in 1.5 mL C_6D_6.

$^{31}P\{^1H\}$ NMR (C_6D_6, 161 MHz): ∂ -0.97 (d, $^2J_{PN}$ = 19.27 Hz) and 22.08 (d, $^2J_{PN}$ = 11.06 Hz).

^{15}N NMR (C_6D_6, 60 MHz): δ -23.2 ($^2J_{PN}$ = 19.27 Hz, $^1J_{NSi}$ = 3.01 Hz) and at δ 291.2 ($^2J_{PN}$ = 11.06 Hz, $^1J_{NSi}$ = 2.01 Hz).

4.7 References.

[1] Jolly, W. L., Inorganic Chemistry of Nitrogen, W. A. Benjamin Inc, New York, New York, 1964, p. 4.

[2] Burgess, B. K.; Lowe, D.J. *Chem. Rev.* **1996**, *96*, 2983.

[3] MacKay, B. A.; Fryzuk, M. D. *Chem. Rev.* **2004**, *104*, 385.

[4] Fryzuk, M. D.; Shaver, M. P. *Adv. Synth. Catal.* **2003**, *345*, 1061.

[5] Stoicheff, B. P. *Can. J. Phys.* **1954**, *32*, 630.

[6] Bouwstra, J. A.; Schouten, A.; Kroon, J. *Acta Cryst. C.* **1983**, *39*, 1121.

[7] Collin, R. L.; Libscomb, W. N. *Acta Cryst.* **1951**, *4*, 10.

[8] de la Jara Real, A.; Tenorio, M. J.; Puerta, M. C.; Valerga, P. *Organometallics* **1995**, *14*, 3839.

[9] Fryzuk, M. D.; Haddad, T. S.; Rettig, S. J. *J. Am. Chem. Soc.* **1990**, *112*, 8185.

[10] Hanna, T. E.; Bernskoetter, W. H.; Bouwkamp, M. W.; Lobkovsky, E.; Chirik, P. J. *Organometallics*, **2007**, *26*, 2431.

[11] Evans, W. J.; Lee, D. S.; Ziller, J. W. *J. Am. Chem. Soc.*, **2004**, *126*, 454.

[12] Sita, L. R.; Hirotsu, M.; Fontaine, P. P.; Epshteyn, A.; Zavalij, P. Y. *J. Am. Chem. Soc.*, **2007**, *129*, 9284.

[13] Arnold, J.; Chomitz, W. A. *Chem. Commun.*, **2007**, *45*, 4797.

[14] Lee, D. W.; Kaska, W. C.; Jensen, C. M. *Organometallics*, **1998**, *17*, 1.

[15] Pool, J. A.; Lobkovsky, E.; Chirik, P. J. *Nature* **2004**, 527.

[16] Gambarotta, S.; Dubé.; Yap, G. P. A. *Organometallics*, **2000**, *19*, 4820.

[17] Chirik, P. J.; Bernskoetter, W. H.; Olmos, A. V.; Lobkovsky, E. *Organometallics* **2006**, *125*, 1021.

[18] Fryzuk, M. D.; Johnson, S. A. *Coord. Chem. Rev.* **2000**, *200-202*, 279.

[19] **A:** Rocklage, S. M.; Turner, H. W.; Fellmann, J. D.; Schrock, R. R.; *Organometallics* **1982**, *1*, 703.

[20] **B:** Fryzuk, M. D.; Haddad, T. S.; Rettig, S. J. *J. Am. Chem. Soc.*, **1990**, *112*, 8185.

[21] **C:** Duchateau, R.; Gambarotta, S.; Beydoun, N.; Bensimon, C. *J. Am. Chem. Soc.* **1991**, *113*, 8986.

[22] **D:** Hirotsu, M.; Fontaine, P. P.; Zavalij, P. Y.; Sita, L. R.; *J. Am. Chem. Soc.* **2007**, *129*, 12690.

[23] **E:** Morello, L.; Yu, P.; Carmichael, D.; Patrick, B. O.; Fryzuk, M. D.; *J. Am. Chem. Soc.* **2005**, *127*, 37.

[24] Fryzuk, M. D. *Chem. Rec.* **2002**, *3*, 2.

[25] Evans, W. J.; Ulibarri, T. A.; Ziller, J. W. *J. Am. Chem. Soc.* **1988**, *110*, 6877.

[26] Fomitchev, D. V.; Bagley, K. A.; Coppens, P. *J. Am. Chem. Soc.* **2000**, *122*, 532.

[27] Allen, A. D.; Senoff, C. V. *J. Chem. Soc. Chem. Commun.* **1965**, *24*, 621.

[28] Burgess, B. K. *Chem. Rev.* **1990**, *90*, 1377.

[29] Sellmann, D.; Sutter, J. *Acc. Chem. Res.* **1997**, *30*, 460.

[30] Einsle, O.; Tezcan, F. A.; Andrade, S. L. A.; Schmid, B.; Yoshida, M.; Howard, J. B.; Rees, D. C. *Science* **2002**, *297*, 1696.

[31] Huniar, U.; Ahlrichs, R.; Coucouvanis, D. *J. Am. Chem. Soc.* **2004**, *126*, 2588.

[32] Dance, I. *Chem. Commun.* **2003**, *3*, 324.

[33] Hinnemann, B.; Norskov, J. K. *J. Am. Chem. Soc.* **2004**, *126*, 3920.

[34] Lovell, T.; Liu, T.; Case, D. A.; Noodleman, L. *J. Am. Chem. Soc.* **2003**, *125*, 8377.

[35] Yang, T.C.; Maeser, N. K.; Laryukhin, M.; Lee, H. I.; Dean, D. R.; Seefeldt, L. C.; Hoffman, B. M. *J. Am. Chem. Soc.* **2005**, *127*, 12804.

[36] Lee, H. I.; Benton, P. M. C.; Laryukhin, M.; Igarashi, R. Y.; Dean, D. R.; Seefeldt, L. C.; Hoffman, B. M. *J. Am. Chem. Soc.* **2003**, *125*, 5604.

[37] Postgate, J. *Nitrogen Fixation*; Cambridge Press: Cambridge, 1998.

[38] Fryzuk, M. D. *Nature* **2004**, *427*, 498.

[39] Fryzuk, M. D.; Johnson, S. A.; Rettig, S. J. *J. Am. Chem. Soc.* **1998**, *120*, 11024.

[40] Fryzuk, M. D.; Johnson, S. A.; Patrick, B. O.; Albinati, A.; Mason, S. A.; Koetzle, T. F. *J. Am. Chem. Soc.* **2001**, *123*, 3960.

[41] de Wolf, J. M.; Blaauw, R.; Meetsma, A.; Teuben, J. H.; Gyepes, R.; Varga, V.; Mach, K.; Veldman, N.; Spek, A. L. *Organometallics* **1996**, *15*, 4977.

[42] Akagi, F.; Matsuo, T.; Kawaguichi, H. *Angew. Chem. Int. Ed.*, **2007**, *46*, 8778.

[43] Bianchini, C.; Meli, A.; Perruzzini, M.; Vizza, F.; Zanobini, F. *Organometallics* **1989**, *8*, 2080.

[44] Chaudret, B.; Devillers, J.; Poilblanc, R. *Organometallics* **1985**, *4*, 1727.

[45] Fryzuk, M. D.; MacKay, B. A.; Johnson, S. A.; Patrick, B. O. *Angew. Chem. Int. Ed.*, **2002**, *41*, 3709.

[46] MacKay, B. A.; Johnson, S. A.; Patrick, B. O.; Fryzuk, M. D. *Organometallics* **2005**, *24*, 3836.

[47] Fryzuk, M. D.; MacKay, B. A.; Patrick, B. O. *J. Am. Chem. Soc.* **2003**, *125*, 3234.

Chpt 2

[48] Siegbahn, P. E. M. *J. Am. Chem. Soc.* **1993**, *115*, 5803.

[49] Crabtree, R. H. *The Organometallic Chemistry of the Transition Metals 4th Ed.*, John Wiley & Sons: New Jersey, **2004**.

[50] Henrici-Olivé, G.; Olivé, S. *Topics in Current Chemistry*, Springer: Berlin, **1976**.

[51] Thorn, D. L.; Hoffmann, R. *J. Am. Chem. Soc.* **1978**, *100*, 2079.

[52] Koga, N.; Jin, *S.*-Q.; Morokuma, K. *J. Am. Chem. Soc.* ***1988***, *110*, 3417.

[53] Fukui; K.; Inagaki, S. *J. Am. Chem. Soc.* **1975**, *97*, 4445.

[54] Koga, N.; Morokuma, K. *Chem. Rev.* **1991**, *91*, 823.

[55] Decker, S. A.; Cundari, T. R. *New J. Chem.* **2002**, *26*, 129.

[56] Shiotsuki, M.; White, P. S.; Brookhart, M.; Templeton, J. L. *J. Am. Chem. Soc.* **2007**, *129*, 4058.

[57] Burger, B. J.; Santarsiero, B. D.; Trimmer, M. S.; Bercaw, J. E. *J. Am. Chem. Soc.* **1988**, *110*, 3134.

[58] Gérard, H.; Eisenstein, O. *Dalton Trans.* **2003**, *5*, 839.

[59] Brookhart, M; Hauptman, E; Lincoln, D. M. *J. Am. Chem. Soc.*, **1992**, *114*

[60] Crabtree, R. *Acc. Chem. Res.* **1979**, *12*, 331.

[61] Shapiro, P. J.; Cotter, D. W. Schaefer, W. P.; Labinger, J. A.; Bercaw, J. E. *J. Am. Chem. Soc.* **1994**, *116*, 4623.

[62] Okuda, J.; Voth, P.; Arndt, S.; Spaniol, T. P.; Green, M. L.; Ackerman, L. J. *Organometallics*, **2003**, *22*, 65.

[63] Casey, C. P.; Tunge, J. A.; Lee, T. Y.; Carpenetti II, D. W. *Organometallics*, **2002**, *21*, 389.

[64] Labinger, J. A.; Schwartz, J. *Angew. Chem. Int. Ed. Engl.* **1976**, *15*, 333.

[65] Hart, D. W.; Schwartz, J. *J. Am. Chem. Soc.* **1974**, *96*, 8115.

[66] Bertelo, C. A.; Schwartz, J. *J. Am. Chem. Soc.* **1976**, *98*, 262.

[67] Schwartz, J.; Blackburn, T. F.; Labinger, J. A. *Tetrahedron Lett.* **1975**, 3041.

[68] Baldwin, J. E.; Almog, J.; Huff, J. *J. Am. Chem. Soc.* **1975**, *97*, 228.

[69] Fryzuk, M. D.; Johnson, S. A.; Patrick, B. O.; Albinati, A.; Mason, S. A.; Koetzle, T. F. *J. Am. Chem. Soc.* **2001**, *123*, 3960.

[70] Pool, J. A.; Chirik, P. J. *Can. J. Chem.*, **2005**, *83*, 286.

[71] Shilov, A. E.; Borodko, Y. G.; Ivleva, I. N.; Kachapina, L. M.; Salienko, S. I.; Shilova, A. K. *J. C. S. Chem. Commun.*, **1972**, *21*, 1178.

[72] Manriquez, J. M.; Bercaw, J. E. *J. Am. Chem.*, **1974**, *96*, 6229.

[73] Sanner, R. D.; Manriquez, J. M.; Marsh, R. E.; Bercaw, J. E. *J. Am. Chem. Soc.*, **1976**, *98*, 8351.

[74] Pool, J. A.; Lobkovsky, E.; Chirik, P. J. *Nature*, **2004**, *427*, 527.

[75] de Wolf, J. M.; Blaauw, R.; Meetsma, A.; Teuben, J. H.; Gyepes, R.; Varga, V.; Mach, K.; Veldman, N.; Spek, A. L. *Organometallics,* **1996**, *15*, 4977.

[76] Sanner, R. D.; Duggan, M. D.; McKenzie, T. C.; Marsh, R. E.; Bercaw, J. E. *J. Am. Chem. Soc.*, **1976**, *98*, 8358.

[77] Hanna, T. E.; Bernskoetter, W. H.; Bouwkamp, M. W.; Lobkovsky, E.; Chirik, P. J. *Organometallics*, **2007**, *26*, 2431.

[78] Bregel, D. C.; Oldham, S. M.; Lachicotte, R. J.; Eisenberg, R. *Inorg. Chem.*, **2002**, *41*, 4371.

[79] Pool, J. A.; Lobkovsky, E.; Chirik, P. J. *J. Am. Chem. Soc.*, **2003**, *125*, 2241.

[80] Chirik, P. J.; Henling, L. M.; Bercaw, J. E. *Organometallics*, **2001**, *20*, 534.

[81] Hanna, T. E.; Keresztes, I.; Lobkovsky, E.; Chirik, P. J. *Inorg. Chem.* **2006**, *46*, 1675.

[82] Bernskoetter, W. H.; Olmos, A. V.; Lobkovsky, E.; Chirik, P. J. *Organometallics*, **2006**, *25*, 1021.

[83] Soloveichik, G. L.; Bulychev, B. M. *Russ. Chem. Rev.*, **1982**, *51*, 286.

[84] Curtis, D. M.; Bell, L. G.; Butler, W. M. *Organometallics*, **1985**, *4*, 701.

[85] Moore, D. S.; Robinson, S. D. *Chem. Soc. Rev.*, **1983**, *12*, 415.

[86] Parshall, G. W.; Tebbe, F. N. *J. Am. Chem. Soc.*, **1971**, *93*, 3793.

[87] Parshall, G. W.; Tebbe, F. N.; Barefield, E. K. *J. Am. Chem. Soc.*, **1970**, *92*, 5234.

[88] Antiñolo, A.; Hermosilla-Carrillo, F.; Fajardo, M.; Fernández-Baeza, J.; Garcia-Yuste, S.; Otero, A. *Coord. Chem. Rev.*, **1999**, *193-195*, 43.

[89] Fryzuk, M. D.; MacKay, B. A.; Johnson, S. A.; Patrick, B. O. *Angew. Chem. Int. Ed.*, **2002**, *41*, 3709.

[90] MacKay, B. A.; Johnson, S. A.; Patrick, B. O.; Fryzuk, M. D. *Can. J. Chem.*, **2005**, *83*, 315.

[91] MacKay, B. A.; Patrick, B. O.; Fryzuk, M. D. *Organometallics*, **2005**, *24*, 3836.

[92] Fryzuk, M. D.; MacKay, B. A.; Patrick, B. O. *J. Am. Chem. Soc.*, **2003**, *125*, 3234.

[93] Spencer, L. P.; MacKay, B. A.; Patrick, B. O.; Fryzuk, M. D. *Proc. Nat. Acad. Sci.*, **2006**, *103*, 17094.

[94] Fryzuk, M. D.; Ohki, Y. *Angew. Chem. Int. Ed.*, **2007**, *46*, 3180.

[95] Sita, L. R.; Hirotsu, M.; Fontaine, P. P.; Zavallij, P. Y. *J. Am. Chem. Soc.*, **2007**, *129*, 12690.

[96] Shaver, M. P.; Fryzuk, M. D. *Organometallics*, **2001**, *24*, 1419.

[97] Courtenay, S. S.; Stephan, D. W. *Organometallics*, **2005**, *20*, 1442

[98] Yue, N.; Hollink, E.; Guérin, F.; Stephan, D. W. *Organometallics*, **2001**, *20*, 4424.

[99] Chirik, P. J. *Dalton Trans.*, **2007**, *1*, 16.

[100] Parshall, G. W.; Tebbe, F. N.; Barefield, E. K. *J. Am. Chem. Soc.*, **1970**, *92*, 5234.

[101] Parshall, G. W.; Tebbe, F. N. *J. Am. Chem. Soc.*, **1971**, *93*, 3793.

[102] Beweries, T.; Burlakov, V. V.; Bach, M. A.; Arndt, P.; Baumann, W.; Spannenberg, A.; Rosenthal, U. *Organometallics*, **2007**, *26*, 247.

[103] Fryzuk, M. D.; Johnson, S. A.; Patrick, B. O.; Albinati, A.; Mason, S. A.; Koetzle, T. F. *J. Am. Chem. Soc.* **2001**, *123*, 3960.

[104] Fryzuk, M. D.; Johnson, S. A. *Coord. Chem. Rev.*, **2000**, *200-202*, 379.

[105] Fryzuk, M. D. *Chem. Rec.*, **2003**, *3*, 2.

[106] Shaver, M. P.; Fryzuk, M. D. *Adv. Synth. Catal.*, **2003**, *345*, 1061.

[107] Yandulov, D. V.; Schrock, R. R. *Science*, **2003**, *301*, 76.

[108] Le Guennic, B.; Kirchner, B.; Reiher, M. *Chem. Eur. J.*, **2005**, *11*, 7448.

[109] Takagahara, K.; Ishino, H.; Ishii, Y.; Hidai, M. *Chem. Lett.*, **1998**, 897.

[110] Takahashi, T.; Kodama, I.; Watakabe, A.; Uchida, Y.; Hidai, M. *J. Am. Chem. Soc.*, **1983**, *105*, 1680.

[111] Ishino, H.; Ishii, Y.; Hidai, M. *Chem. Lett.*, **1998**, 677.

[112] Chatt, J.; Heath, G. A.; Leigh, G. J. *J. Chem. Soc. Chem. Commun.*, **1972**, 444.

[113] Chatt, J.; Diamantis, A. A.; Heath, G. A.; Hooper, N. E.; Leigh, G. J. *J. Chem. Soc. Dalton. Trans.*, **1977**, 688.

[114] Hidai, M.; Komori, K.; Kodama, T.; Jin, D. M.; Takahashi, T.; Sugiura, S.; Uchida, Y.; Mizobe, Y. *J. Organomet. Chem.*, **1984**, *272*, 155.

[115] O'Donoghue, M. B.; Davis, W. M.; Schrock, R. R. *Inorg. Chem.*, **1998**, *37*, 5149.

[116] Studt, F.; MacKay, B. A.; Johnson, S. A.; Patrick, B. O.; Fryzuk, M. D.; Tuckzek, F. *Chem. Eur. J.*, **2005**, *11*, 604.

[117] Clentsmith, G. K. B.; Bates, V. M. E.; Hitchcock, P. B.; Cloke, F. G. N. *J. Am. Chem. Soc.*, **1999**, *121*, 10444.

[118] Kawaguchi, H.; Matsuo, T. *Angew. Chem. Int. Ed.*, **2002**, *41*, 2792.

[119] Fryzuk, M. D.; MacKay, B. A.; Johnson, S. A.; Patrick, B. O. *Angew. Chem. Int. Ed.*, **2002**, *41*, 3709.

[120] Jutzi, P.; Neumann, B.; Reumann, G.; Stammler, H. G. *Organometallics*, **1998**, *17*, 1305.

[121] Fryzuk, M. D.; Johnson, S. A.; Patrick, B. O.; Albinati, A.; Mason, S. A.; Koetzle, T. F. *J. Am. Chem. Soc.* **2001**, *123*, 3960.

Appendix

Table A-1. Crystallographic Data and Structure Refinement for $([NPN]Ta)_2(\mu\text{-}H)_4$ (**2**) and $([NPN]Ta(CH_2)_5CH_3)_2(\mu\text{-}\eta^1\text{:}\eta^1\text{-}N_2)$ (**11**).

	$([NPN]Ta)_2(\mu\text{-}H)_4$ (**2**)	$([NPN]Ta(CH_2)_5CH_3)_2(\mu\text{-}\eta^1\text{:}\eta^1\text{-}N_2)$ (**11**)
Empirical formula	$C_{48}H_{66}N_4P_2Si_4Ta_2$	$C_{60}H_{88}N_6P_2Si_4Ta_2$
Formula weight	1235.25	1429.56
Colour, habit	purple, tablet	red, prism
Crystal size, mm	0.22 × 0.13 × 0.03	0.10 × 0.22 × 0.31
Crystal system	triclinic	triclinic
Space group	P-1	P-1
a, Å	11.140(5)	11.658(4)
b, Å	13.744(5)	11.918(5)
c, Å	18.708(5)	12.911(7)
α, deg	86.215(5)	105.49(3)
β, deg	87.146(5)	100.10(2)
γ, deg	66.143(5)	90.47(2)
Z	2	2
ρ_{calc}, g/cm^3	1.570	1.397
F(000)	1228	722
radiation	Mo	Mo
$2\theta_{max}$, deg	56.02	54.21
total no. of reflections	51577	30810
no. of unique reflections	12539	8132
R_{merge}	0.0333	0.0376
no. with $I \geq n\theta(I)$	12539	8132
no. of parameters	557	334
R (F^2, all data)	0.0223	0.0285
R_w (F^2, all data)	0.0474	0.0912
R (F, I>nσ(I))	0.0364	0.0322
R_w (F, I>nσ(I))	0.0510	0.0936
gof	0.979	1.125
residual dens, e/Å^3	1.076, -1.012	3.132, -0.865

R_1 (F^2, I>2σ(I)) = $\Sigma \; || F_o|-|F_c|| / \Sigma |F_o|$; R_w (all data) = $(\Sigma w(|F_o^2|-|F_c^2|)^2 / \Sigma w|F_o^2|^2)^{1/2}$

Table A-2. Crystallographic Data and Structure Refinement for [N(μ-P=N)N]Ta(μ-H)$_2$(μ-N(HfCp$_2$))Ta[NPN] (**14**) and [(PhNH)(NPμ-N)Ta]$_2$ (**19**).

	[N(μ-P=N)N]Ta(μ-H)$_2$(μ-N(HfCp$_2$))Ta[NPN] (**14**)	[(PhNH)(NPμ-N)Ta]$_2$ (**19**)
Empirical formula	$C_{70}H_{86}Hf_1N_6P_2Si_4Ta_2$	$C_{48}H_{62}N_6P_2Si_4Ta_2$
Formula weight	1726.14	1259.24
Colour, habit	purple, needle	yellow, chip
Crystal size, mm	0.24 × 0.56 × 0.10	0.45 × 0.50 × 0.26
Crystal system	triclinic	triclinic
Space group	P-1	P1
a, Å	13.4808(14)	9.2542(15)
b, Å	14.8372(13)	11.3559(18)
c, Å	17.7810(19)	13.367(2)
α, deg	81.516(4)	70.398(8)
β, deg	87.329(5)	78.401(7)
γ, deg	82.437(4)	81.041(7)
Z	2	1
ρ_{calc}, g/cm^3	1.645	1.620
F(000)	1704	624
radiation	Mo	Mo
$2\theta_{max}$, deg	55.8	50.3
total no. of reflections	14440	22423
no. of unique reflections	12837	5927
R_{merge}	0.0846	0.0262
no. with $I \geq n\theta(I)$	12837	5927
no. of parameters	782	284
R (F^2, all data)	0.0333	0.0145
R_w (F^2, all data)	0.0792	0.0339
R (F, I>nσ(I))	0.0501	0.0162
R_w (F, I>nσ(I))	0.0860	0.0345
gof	1.075	1.047
residual dens, e/Å^3	1.628, -0.915	0.422, -0.378

R_1 (F^2, I>2σ(I)) = $\Sigma \; || F_o|-|F_c|| / \Sigma |F_o|$; R_w (all data) = $(\Sigma w(|F_o^2|-|F_c^2|)^2 / \Sigma w|F_o^2|^2)^{1/2}$